AMES LABORATORY Energy & Mineral Resources Research Institute
Iowa State University | Ames, Iowa 50011

Item I

August 2, 1984

COPY

Mr. Goutam Bagchi, Leader
Seismic Qualification Section
Office of Nuclear Reactor Regulation
U.S. Nuclear Regulatory Commission
Phillips Building, P-234
7920 Norfolk Avenue
Bethesda, MD 20034

SUBJECT: Summary Report for Ames Laboratory Technical Assistance to the Division of Engineering, Nuclear Reactor Regulation--"Leakage Characteristics of Nuclear Containment Hatches During a Severe Accident" FIN NO. A4135-4

Dear Goutam:

Enclosed, please find a brief summary report on the findings of our study of the Sequoyah equipment hatch. A draft of the complete report will be mailed later in August.

If you have any questions, please call.

Sincerely,

Lowell Greimann/cb

Lowell Greimann
Senior Engineer

LG:cb

Enclosure

cc: Delwyn Bluhm
Ames Laboratory

Tom Bridges
EG&G, Idaho, Inc.

Charles Hofmayer
Brookhaven National Labs

Operated for the U.S. Department of Energy Under Contract W-7405-Eng-82

I

SEQUOYAH EQUIPMENT HATCH SEAL LEAKAGE

L. Greimann, F. Fanous, D. Bluhm

July 1984

SUMMARY

The following summary constitutes an abstract of a soon-to-be-published report by the same title in which complete details of the analysis are presented.

Background and Objective

As part of the Containment Performance Working Group study, an analytical effort was undertaken to investigate the leakage characteristics of the Sequoyah equipment hatch seal during severe accidents. The effects of containment deformation and hatch postbuckling on the distortions at the sealing surface were to be included. Only leakage at the seal surface is considered in this work. Leakage through a crack in the steel plate was not considered.

Equipment Hatch Model

The equipment hatch is one of several penetrations in the Sequoyah containment vessel. If penetration effects are neglected, gross yielding of the 1/2-inch shell plate near the springline will occur at a pressure of 50 to 60 psig. A three-dimensional finite element model of the equipment hatch was developed which includes: shell elements for the hatch, sleeve, containment plate and stiffeners; prestressed bar elements for the swing bolts; and friction elements for the seal interface. One-quarter symmetry of the assembly was enforced. Geometric and material nonlinearities were included. A single lobe imperfection was included in the hatch shell model. The imperfection amplitude was equal to the ASME tolerance allowable and the wave length was equal to the elastic buckling length. Loading which corresponds to pressure inside the containment was applied in increments. Analyses were made with two coefficients of friction for the steel at the seal interface: 0.3 and 0.6.

Results

The maximum strain of about 1.4 percent occurred in the top of the sleeve, near its intersection with the containment. The maximum relative sliding and rotation at the seal interface was 0.9 inch and 1 1/2 degrees, respectively, for the 0.3 friction coefficient. Hatch buckling occurred in the range of 85 to 90 psi.

Conclusions

The Sequoyah equipment hatch seals should not leak before very large strains develop in the 1/2-inch containment shell plate near the springline, which occurs between 50 and 60 psig. In the unlikely event of hatch buckling, postbuckling deformations would not introduce leakage.

Item I

NUREG/CR-3952
IS-4862

AMES LABORATORY

Preliminary

WORKING DRAFT
FOR DISCUSSION PURPOSES ONLY

SEQUOYAH EQUIPMENT HATCH SEAL LEAKAGE

Final Report

August 1984

Prepared by

L. Greimann, F. Fanous, D. Bluhm

Ames Laboratory
Iowa State University
Ames, IA 50011

Prepared for

Division of Engineering
Office of Nuclear Reactor Regulation
U.S. Nuclear Regulatory Commission
Washington, D.C. 20555
NRC FIN NO. A4135-4

NUREG/CR-3952
IS-4862

Preliminary

SEQUOYAH EQUIPMENT HATCH SEAL LEAKAGE

Final Report

August 1984

Prepared by

L. Greimann, F. Fanous, D. Bluhm

Ames Laboratory
Iowa State University
Ames, IA 50011

Prepared for

Division of Engineering
Office of Nuclear Reactor Regulation
U.S. Nuclear Regulatory Commission
Washington, D.C. 20555
NRC FIN NO. A4135-4

DISCLAIMER

Printed in the United States of America

Available from
National Technical Information Service
U.S. Department of Commerce
5265 Port Royal Road
Springfield, VA 22161

TABLE OF CONTENTS

LIST OF FIGURES

ACKNOWLEDGMENT

The authors would like to express their appreciation for three members of the U.S. Nuclear Regulatory Commission, Mr. Goutam Bagchi, Leader, Seismic Qualification Section; Mr. Vince Noonan, Chief, Equipment Qualifications Branch; and, Mr. Robert Wright, NRC Project Manager, for their help throughout the course of this work. Mr. Charles Hofmayer of Brookhaven National Laboratory and Mr. Tom Bridges of EG&G, Idaho, Inc., supplied information which was very useful for the conduct of this work. The authors also wish to acknowledge the able assistance of the project secretaries, Connie Bates and Beth Lott, for the word processor operations and the secretarial services associated with this project.

EXECUTIVE SUMMARY

Nuclear containments, which will not leak during a design accident, may leak during a severe accident when the pressure increases beyond the design level. Small leaks which are visualized as occurring at local details may occur before complete vessel failure. As part of the NRC Containment Performance Working program, this study was undertaken to investigate the leakage-before-break potential of a typical equipment hatch seal. Buckling of the hatch door, large deformations and ovaling of the hatch sleeve are potential causes of mismatch at the sealing surface which can result in a leakage path.

Among the several plants being considered by the Containment Performance Working Group, the Sequoyah equipment hatch was selected. If penetrations effects are neglected, gross yielding of the 1/2-inch shell plate near the springline of the Sequoyah containment will occur at an internal pressure of between 50 and 60 psi.

The effect of an imperfection on the buckling strength of the hatch was first studied using an axisymmetric model of the hatch, containment and sleeve. A single axisymmetric imperfection lobe (cosine curve) was placed at the crown and adjacent to the seal. The buckling load for various values of the imperfection wave length and amplitutde was calculated using the BOSOR5 code. The nonlinear behavior of the material was approximated by a piecewise linear relationship which accounted for residual stress effects. The critical value of the imperfection wave length, amplitude and location was selected to be used in a three-dimensional finite element model.

The ANSYS finite element computer code was used to perform a three-dimensional finite element analysis of the containment/sleeve/hatch assembly. One-quarter symmetry is assumed about the hatch vertical and horizontal diameters. The hatch system was modeled using flat triangular shell elements for the door, sleeve, containment, ring stiffeners and stringers. Prestressed bar elements were used to model the swing bolts and friction elements were employed to idealize the seal interface. Geometric and material nonlinear behavior were also included. The model was analyzed twice, using coefficients of friction of 0.6 and 0.3. In both analyses the pretension forces in the swing bolts were first applied and then the internal pressure was increased in increments as convergence was insured.

The results of the finite element analysis showed that a maximum of 0.9 inch of relative sliding occurred at the seal interface at 82 psi. The maximum relative rotation of the sealing surfaces was 1-1/2 degrees. The buckling load was predicted to occur in the range of 85 to 90 psi, but postbuckling displacements did not cause large seal motions.

In conclusion, the Sequoyah equipment hatch should not leak before very large strains develop in the 1/2-inch containment shell plate near the springline, which occurs between 50 and 60 psi. In the unlikely event of hatch buckling, postbuckling deformations would not introduce leakage.

1. INTRODUCTION

1.1 Background

Nuclear containments are designed to prevent leakage of radioactive material. As the pressure and temperature increase during a severe accident, which is beyond the design level, the containment may reach a point where leakage begins to occur. There are at least two models used to characterize this leakage--the threshold model and the leak-before-break model.

In the threshold model, the containment is assured to be leak-tight until certain pressure/temperature conditions are reached. At this point, a very large rupture or burst area is postulated and large quantitites of fission products are released. Typically, the predicted threshold pressure is based upon a model of the containment shell which only permits such gross failure modes. Local discontinuities, e.g., penetrations, hatches, seals, are usually omitted from such models [1.1].

As an alternative model, the leak-before-break model is probably more realistic. In this model, it is hypothesized that small leak paths will develop as the containment is being pressurized at levels below the threshold. Hence, pressure is being released at earlier stages and the threshold pressure may never be reached. Typically, these small leaks are visualized as occurring at local details, e.g., penetrations, hatches, and seals which are often omitted from the threshold model.

The NRC has established a Containment Performance Working Group (CPWG), at the request of the Severe Accident Research Plan (SARP) Senior Review Group, to develop containment leakage models. Besides the containment loads aspect of this problem, this group is studying containment leakage in several categories. The current hypothesis of the group is that leakage will, most likely, begin at certain penetrations or other discontinuities (leak-before-break) and not by gross rupture of the containment shell. As a test for this hypothesis, the group is currently involved in quantifying predictions of the amount of leakage which may occur in six representative containments.

1.2 Objective

The objective of this particular work is to investigate the leak-before-break potential of a typical equipment hatch seal. The results will be incorporated into the work of the entire Containment Performance Working Group.

In the initial stages of the work, postbuckling and other large displacements of the equipment hatch shell itself were considered to be possible causes of leakage as local deformations distorted the sealing surface. As the project and communication with others involved in similar work developed, another possibility became evident--ovaling of the penetration sleeve. That is, as the containment shell is

pressurized, circumferential stresses in the containment tend to distort the hole and sleeve for the equipment penetration into an elliptical shape with a horizontal major axis. This distortion causes a mismatch of the sealing surface with leakage potential. (This behavior is documented and described more fully herein.)

2. EQUIPMENT HATCH DESCRIPTION

2.1 Hatch Selection

There are many different equipment hatch configurations in existing containments. Since an initial consideration was postbuckling displacement, a hatch under compression was selected (pressure seating) as opposed to a hatch in tension (pressure unseating). Again, since buckling was important, it was decided to select a hatch with the most likely possibility of buckling, i.e., a large r/t value. From the six plants being studied by the Containment Performance Working Group, the Sequoyah equipment hatch was selected.

2.2 Geometry and Materials

The Sequoyah equipment hatch is located on Azimuth 285° at Elevation 741' 1 1/2" of the containment (Fig. 2.1). More geometric details of the containment in the vicinity of the hatch are shown in Figs. 2.2, 2.3 and 2.4. Of particular interest in these figures are:

(1) The containment shell is 1/2 inch thick just below the springline. Previous studies [2.1] using axisymmetric (threshold type) models of the Sequoyah containment which neglect penetrations and other nonsymmetric discontinuities, predict shell failure in the 1/2 inch plate at a static pressure between 50 and 60 psig. (The variation in this value is the result of different approaches by the different investigations.)

(2) There is 5/8 inch shell plate in the immediate vicinity of the equipment hatch penetration (Fig. 2.2). The local plate thickness of 1-1/2 inch is presumably used to satisfy the ASME area replacement rule.

(3) The sleeve length between the containment wall and the sealing surfaces is only 14.5 inches at the horizontal diameter of the sleeve. This distance is quite short and, as will be seen, couples the containment and hatch shell deformations.

(4) The actual containment in the upper right quadrant of the hatch region is shown in Fig. 2.2, except a ring actually located at Elevation 740' 6 5/8" was moved to the hatch centerline to introduce symmetry. The containment in the remaining three quadrants is not symmetrical, e.g., the 5/8 inch plate does not exist in the same locations in the other quadrants.

Shell geometric imperfections have a significant effect on buckling strength. Particularly for spherical shells under external pressure, small deviations from perfect sphericity greatly reduce the buckling strength below classical buckling theory. Figure 2.5 illustrates the ASME tolerance criteria on shell imperfections [2.2]. For the Sequoyah hatch, the maximum deviation from a perfect circular arc, e, is

permitted to be one shell thickness (3/4 inch) over a chord length of 67 inches.

The details of the seals as furnished by TVA are shown in Fig. 2.6. Compression set values (ASTM D 395) for typical temperature/radiation loadings are also listed.

The containment steel is A516, Grade 60 with a specified minimum yield of 32 ksi. Actual mill test yield strengths for typical plates with the various thicknesses are listed in Fig. 2.7. Residual stresses have a significant affect on the buckling strength of steel components. When regions with residual stress yield, the material tangent modulus is reduced and the structural tangent stiffness is, thereby, reduced. In lieu of knowing the actual initial residual stress pattern, this effect can be approximated by using an effective stress-strain curve with a proportional limit below the yield strength [2.4, 2.5]. For the present case, the proportional limit will be taken as one-half yield which approximates residual stresses of the order of one-half yield. For each thickness, the stress-strain curve is approximated by a modified Ramberg-Osgood equation [2.2] with a strain hardening exponent n of five (Fig. 2.7). For purposes of the following analysis, this curve is approximated by a piecewise linear curve.

3. IMPERFECTION STUDY

As mentioned previously, imperfections in the spherical cap hatch can have a large effect on its buckling behavior. To study this effect in an economical manner, an axisymmetric model of the hatch and sleeve was developed for BOSOR5 [3.1]. Since the model is axisymmetric, the cylindrical containment was approximated by a portion of a sphere (Fig. 3.1). No relative motion was permitted at the sealing surface.

A single axisymmetric imperfection lobe (cosine curve) was placed at the crown (Fig. 3.2) and adjacent to the flange (Fig. 3.3). BOSOR5 was executed to calculate the buckling load for various valves of the imperfection wave length, L_o, and amplitude. The resulting buckling pressures are plotted in Figs. 3.4 and 3.5, respectively. The critical buckling length for classical elastic buckling of a perfect sphere is approximately [3.2]

$$L_{cr} = 3.5\sqrt{rt} = 47 \text{ in.} \qquad (3.1)$$

Figure 3.4 illustrates that this is approximately the wave length of the crown imperfection which minimizes the buckling strength of the Sequoyah hatch. The length of the (axisymmetric) imperfection adjacent to the flange has little effect on buckling strength. As expected, Fig. 3.5 confirms that an increasing imperfection amplitude decreases buckling strength. Note again that the maximum permitted value of e for the Sequoyah hatch is 3/4 inch (see Sec. 2.3).

The "design" buckling pressure for the hatch as calculated from the ASME Code, Case N-284 [3.3] is 50 psi. (In terms of Case N-284, the capacity reduction factor is 0.146 ($M = 240/\sqrt{(140)(0.75)} = 17.9$), the classical elastic buckling pressure is 343 psig and the plasticity reduction factor is 1.0, i.e., elastic buckling.) This value is shown in Fig. 3.5. Note that a large imperfection is necessary to reduce the buckling load to that of the design equations.

For the subsequent three-dimensional analysis, a single imperfection lobe was used with a length, L_o, of 47 inches and a deviation for perfect circularity, e, of 3/4 inch (Fig. 3.6). The imperfection was also assumed to be L_o in the circumferential direction, on the basis that this shape will be sympathetic with the elastic buckling mode in which n lobes form around the circumference. (BOSOR5 indicated n was about 8 for this case [3.4].) The imperfection was located near the flange to maximize its effect on possible distortion at the sealing surface. In anticipation of the possible ovaling effect (Sec. 1.2), compression in the hatch will be largest in the vertical direction. Hence, the imperfection was placed on a vertical diameter.

4. THREE-DIMENSIONAL ANALYSIS

4.1 Model

A three-dimensional finite element model of the Sequoyah equipment hatch was constructed for the ANSYS [4.1] computer program. ANSYS is a general purpose finite element computer program with extensive pre- and post-processing capability. The geometric and material nonlinear analysis capabilities of ANSYS were used in this model. The geometric and material properties presented in Sec. 2.2 and the imperfection in Fig. 3.6 were incorporated into the model. One-quarter symmetry is assumed about the hatch vertical and horizontal diameters, as suggested in Fig. 2.2, even though the containment is only approximately symmetrical.

Symmetry boundary conditions were used in the plane of the vertical and horizontal diameters of the hatch. The model is extended only 20 degrees circumferentially from the meridional plane through the center of the hatch (Fig. 2.2). (This certainty represents a minimum.) Symmetry boundary conditions are also used on this boundary. The top of the model is constrained to move uniformly vertically, i.e., the top of the model remains a plane section.

The mesh in the hatch and sleeve was layed out such that the maximum element dimension was less than $\sqrt{rt}/2$ (6.7 inch for the hatch and 9.5 inch for the sleeve). Flat triangular shell elements were used (STIF48 in ANSYS). The elements in the containment shell are noticeably larger than this guideline ($\sqrt{rt}/2$ of 16 inch), but sufficiently small to approximate its membrane behavior. Rings and stringers were also modeled by shell elements. Figure 4.1 and 4.2 are plots of the finite element mesh from outside and inside the containment, respectively (915 elements, 541 nodes).

The swing bolts which are pretensioned to hold the hatch against the sealing surface (Fig. 2.4) were included in the model as uniaxial, pretensioned bar elements (STIF8). The swing bolts are rigidly connected to the middle surface of the sleeve shell.

The material model is the von Mises yield surface with the Prandtl-Reuss flow rule with isotropic strain hardening. The piecewise linear approximation to the uniaxial stress-strain curve is illustrated in Fig. 2.7.

The interface between the flange and the sleeve is modelled using interface elements (STIF 52) which have friction and opening capability (Fig. 4.3). Normal to the interface, the element is very stiff in compression and very flexible in tension. (Infinite and zero stiffnesses introduce numerical problems.) Tangential to the interface, the element permits relative sliding if the tangential force exceeds the normal (compressive) force multiplied by the coefficient of friction. Two interface elements are used at each nodal meridian of the sleeve--one on the inside and one on the outside of the sleeve.

Such an arrangement permits rotational and sliding discontinuities at the seal interface. (The results to follow illustrate this.) Two different coefficients of friction, 0.6 and 0.3, were used in the analysis of the hatch model. A coefficient of friction of 0.6 represents the clean steel on steel case [4.2].

4.2 Loads and Execution

The finite element model described in the previous section was loaded to correspond to internal pressure on the containment, i.e., pressure on the inside face of the appropriate elements and a vertical load at the top of the model corresponding to the meridional membrane stress resultant in the containment. Two different analysis approaches available in the ANSYS Code were used to analyze the hatch model. A static analysis was performed with the 0.6 coefficient of friction case, while a "slow-dynamic" analysis was used in conjunction with the 0.3 friction coefficient. In both approaches, the prestress in the swing bolts was first applied (25 kips/bolt which is about 1/4 the yield strength) and then the pressure inside the containment was applied.

In the static analysis, the pressure was increased in increments, typically 5 psi. After each increment in pressure was applied, a sufficient number of iterations was run to permit convergence to the nonlinear solution. Convergence criteria were: (1) the change in displacement between consecutive iterations must be less than 0.1 inch and (2) the change in plastic strain divided by the yield strain be less than 0.1. Beyond 80 psi, these criteria were reduced to 0.05 and 0.05, respectively. Through the 82 psi load level, the solution required iterations which used about 55 cpu hours on a VAX 11/780. When the pressure was increased to 84 psi, a zero-stiffness condition occurred, indicating the hatch had buckled at the imperfection. A couple unsuccessful attempts were made to follow the postbuckling behavior using the traditional static analysis.

In an attempt to track the postbuckling behavior with a physically, more realistic analysis, the "slow dynamic" analysis suggested in [4.1] was used for the 0.3 coefficient of friction case. In principle the method is more attractive because the actual buckling process is dynamic. A high damping ratio is used to minimize the vibration response. Physically, this would correspond to placing the hatch in a viscous fluid during pressurization. The pressure in this analysis was increased linearly over a rise time larger than several times the structure natural period (about 1 psi per second). The integration time increments were initially quite large (1 second) as the structure behaved linearly and the high damping produced an essentially static response. As material and geometric nonlinearities began to dominate the problem, the time steps were successively cut in half. For example, a time step of 0.125 seconds was used at 82 psi. At this point, the pressure was increased to 85 psi as a step function and 24 time increments of 0.01 second were run. Since no buckling occurred and since the postbuckling shape is important (not necessarily the buckling pressure), the pressure was stepped to 90 psi and the solution was performed for 100 time steps. During these steps, the time

increment size varied between 0.01 to 0.1 seconds was used. The authors recognize that the larger time step size would yield an inaccurate result, however, it was considered acceptable since the interest was to investigate the postbuckling behavior not to reach a converged solution.

Initially, it was hoped that the time step optimizer within ANSYS may reduce the number of steps and, hence, the amount of cpu time. However, to 82 psi, the "slow-dynamic" required about 70 cpu hours time than the static analysis.

4.3 Results

4.3.1 Prebuckling Results

Typical strain and displacement results are presented in this section. Figure 4.4 will be used to reference the location of the points of interest. Figure 4.5 is a plot of the radial displacement at the center of the hatch, A, the center of the imperfection, B, and the 5/8-inch containment shell plate, C. The displacement at B is the maximum in the model. Strains of interest are plotted in Fig. 4.6. The maximum strain in the hatch occurs at the surface in the imperfection, B. The maximum membrane strain in the containment occurs in the 5/8 inch plate near C. The maximum membrane strain in the entire model occurs in the horizontal direction at the top of the sleeve, D, just outside the containment. Most of the differences between the results for the 0.3 and 0.6 friction cases are caused by the difference in the analysis techniques.

The distortions at the sealing surface can be visualized by examining the deformed shapes at the vertical and horizontal symmetry planes of the hatch, Fig. 4.7 and 4.8, respectively. These figures are plotted for the 0.3 coefficient of friction at 82 psig. Displacements are drawn at an exaggerated scale in these figures. The inset figures in each of these plots are drawn to scale and illustrate the translation and rotation relative to the flange and the flange grooves. These figures and Fig. 4.9 illustrate the ovaling effect, i.e., the forces in the containment shell tend to distort the sleeve into an ellipse. If the frictional forces at the sealing surface where zero, the sleeve would become elliptical and the hatch flange would remain circular with a uniform outward radial motion. This mismatch in shapes causes sliding and rotation at the sealing surface. Friction reduces this mismatch, i.e., tends to force the two surfaces to move together, but it does not eliminate the mismatch.

Figures 4.10 and 4.11 are plots of the vertical displacement in the vertical symmetry plane, F, and the horizontal displacement in the horizontal symmetry plane, G, respectively, at the sealing surface. Down is positive in Fig. 4.10 and to the right is positive in Fig. 4.11. The difference in the displacement for the sleeve and the flange represent the slip at the seal surface. Notice that, as expected, the slip is larger when the coefficient of friction was reduced to 0.3. Figures 4.9 and 4.10 present the rotations at the sealing surface in the vertical and horizontal symmetry planes, respectively. Positive rotations are shown in the inset. Again, the distance between the two

curves represents the relative rotation of the two surfaces. The relative rotation was not much affected by the change in the coefficient of friction.

4.3.2 Postbuckling Results

As previously mentioned, the solution was continued to track the postbuckling behavior of the hatch, especially the seal surface. During the postbuckling process, the radial displacement in the imperfection region continued to grow rapidly compared to the rest of the hatch model. The displacement at the center of the hatch, center of imperfection and the 5/8 inch containment plate are 8.2 inches, 23 inches, and 48 inches, respectively. Despite these large displacements, no noticeable changes in the pre- and postbuckling relative rotation and translation were found. The maximum displacement of 27.8 inches occurred along the vertical symmetry plane in the vicinity of the imperfection region. Figure 4.14 illustrates the unexaggerated deformed shape of the model. Imposed also on Fig. 4.14 is an inset figure drawn to scale illustrating the relative translation and rotation of the flange and flange grooves. The maximum values of the relative sliding and rotation reached during the postbuckling investigation were 1.12 inches and 1.80 degrees, respectively.

4.4 Summary Observations

The maximum strain in the model at 82 psig, for both friction cases, is about 0.014 in the penetration sleeve (Fig. 4.4). Although this strain is probably well below the ultimate strain for the ductile steel used in the containment, the possibility exists that localized plane strain conditions and local flaws may initiate a leakage point. Elastic-plastic fracture mechanics principles could usefully be applied here [4.3].

The maximum relative sliding at the seal surface are:

Coefficient of Friction	Relative Sliding (in.)	Relative Rotation (Degrees)
0.6	0.6	1 1/2
0.3	0.9	1 1/2

With these small amount of displacement of the seals, leakage is very unlikely [4.4]. Even postbuckling displacements did not introduce large displacements at the seals (Sec. 4.3.2).

5. SUMMARY

5.1 Summary

Nuclear containments, which will not leak during a design accident, may leak during a severe accident when the pressure increases beyond the design level. Small leaks which are visualized as occurring at local details may occur before complete vessel failure. As part of the NRC Containment Performance Working program, this study was undertaken to investigate the leakage-before-break potential of a typical equipment hatch seal. Buckling of the hatch door, large deformations and ovaling of the hatch sleeve are potential causes of mismatch at the sealing surface which can result in a leakage path.

Among the several plants being considered by the Containment Performance Working Group, the Sequoyah equipment hatch was selected. If penetrations effects are neglected, gross yielding of the 1/2-inch shell plate near the springline of the Sequoyah containment will occur at an internal pressure of between 50 and 60 psi.

The effect of an imperfection on the buckling strength of the hatch was first studied using an axisymmetric model of the hatch, containment and sleeve. A single axisymmetric imperfection lobe (cosine curve) was placed at the crown and adjacent to the seal. The buckling load for various values of the imperfection wave length and amplitutde was calculated using the BOSOR5 code. The nonlinear behavior of the material was approximated by a piecewise linear relationship which ccounted for residual stress effects. The critical value of the imperfection wave length, amplitude and location was selected to be used in a three-dimensional finite element model.

The ANSYS finite element computer code was used to perform a three-dimensional finite element analysis of the containment/sleeve/hatch assembly. One-quarter symmetry is assumed about the hatch vertical and horizontal diameters. The hatch system was modeled using flat triangular shell elements for the door, sleeve, containment, ring stiffeners and stringers. Prestressed bar elements were used to model the swing bolts and friction elements were employed to idealize the seal interface. Geometric and material nonlinear behavior were also included. The model was analyzed twice, using coefficients of friction of 0.6 and 0.3. In both analyses the pretension forces in the swing bolts were first applied and then the internal pressure was increased in increments as convergence was insured.

The results of the finite element analysis showed that a maximum of 0.9 inch of relative sliding occurred at the seal interface at 82 psi. The maximum relative rotation of the sealing surfaces was 1-1/2 degrees. The buckling load was predicted to occur in the range of 85 to 90 psi, but postbuckling displacements did not cause large seal motions.

5.2 Conclusions

In conclusion, the Sequoyah equipment hatch should not leak before very large strains develop in the 1/2-inch containment shell plate near the springline, which occurs between 50 and 60 psi. In the unlikely event of hatch buckling, postbuckling deformations would not introduce leakage.

5.3 Recommendations

Some of the items which were not included in this study which could be looked at in the future include other hatch imperfections, different friction coefficients and other pretensions in the swing bolts. The analysis methods should continue to be calibrated with existing experimental results, many of which have been published, e.g., shell buckling, pressure vessel experiments. The behavior and the seals with flange separation and rotation needs more study. The effect and temperature gradients on displacements at the seal surface could be important.

High strains in the sleeve, near the containment, should be investigated further. As pressure is increased, leakage will most likely begin at these high strain locations. The potential size of such a path should be studied. Several other penetrations with possibly higher strains should also be considered.

6. REFERENCES

1.1 Greimann, L, Fanous, F., and Bluhm, D., "Containment Analysis Techniques, A State-of-the-Art Summary," Report to Sandia National Laboratory, October 1983.

2.1 Greimann, L., et. al, "Reliability Analysis of Containment Strength, Sequoyah and McGuire Ice Condenser Containments," NUREG/CR-1891, August 1982.

2.2 ASME Boiler and Pressure Vessel Code, Division III.

2.3 Desai, C.S. and Wu, T.H., "A General Function for Stress-Strain Curves," Numerical Methods in Geometrics, ASCE, 1976.

2.4 Brockenbrough, R.L. and Johnston, B.G., Steel Design Manual, U.S. Steel, Pittsburgh, PA, 1974, pg. 47.

2.5 Salmon, C.G. and Johnson, J.E., Steel Structures Design and Behavior, 2nd Edition, Harper and Row, New York, 1980, pg. 263.

3.1 Bushnell, D., "BOSOR5, A Program for Buckling of Elastic-plastic Complex Shells of Revolution Including Large Deflections and Creep," Structural Mechanics Laboratory, Lockheed Missile and Space Co., Palo Alto, CA, 1974.

3.2 Bruch, D.O. and Almarth, B.O., Buckling of Bars, Plates, and Shells, McGraw-Hill, New York, 1975, Chap. 7.

3.3 ASME Boiler and Pressure Vessel Code, Case N-284, "Metal Containment Shell Buckling Design Methods," Supplement #2 to Nuclear Code Case Book, 1980.

3.4 Wackel, N., Jullien, J.F. and Ledermann, P., "Experimental Studies of the Instability of Cylindrical Shells with Initial Imperfections," Recent Advances in Nuclear Component Testing and Theoretical Studies in Buckling, PVP-Vol. 89, ASME, June 17-21, 1984.

4.1 ANSYS Engineering Analysis System, User's Manual and Theoretical Manual, Swanson Analysis Systems, Inc., Houston, PA, 1984 (Version 4.1C).

4.2 Handbook of Chemistry and Physics, 41 Edition, Chemical Rubber Publishing Co., Cleveland, 1960, pg. 2152.

4.3 Idelsohn, S.R., et.al., "Failure Internal Pressure of Spherical Steel Containments," Second Workshop on Containment Integrity, Washington, D.C., June 1984.

4.4 Barnes, B.L., "Containment Penetration Elastomer Seal Test," Second Workshop on Containment Integrity, Washington, D.C., June 1984.

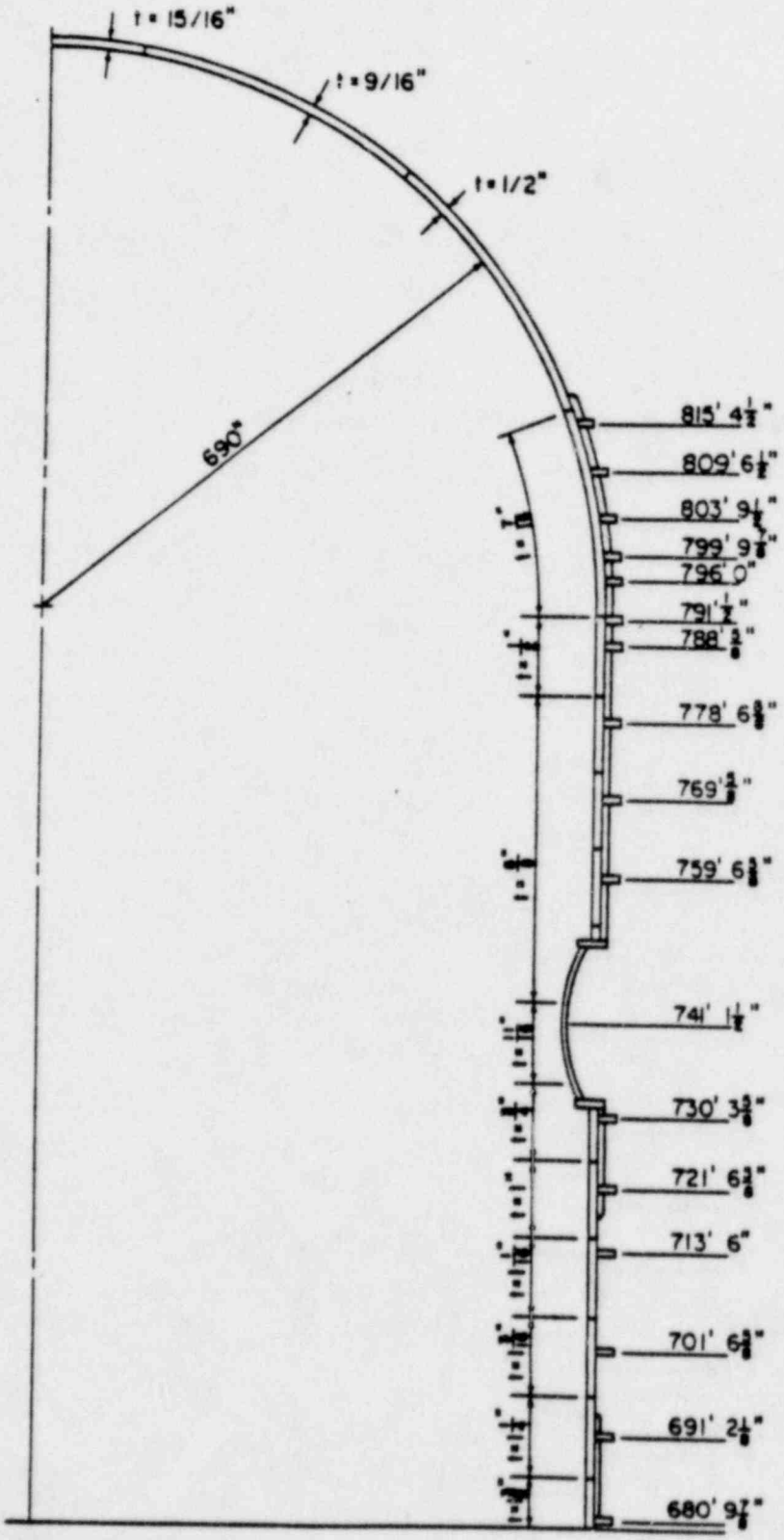

Figure 2.1 Sequoyah Containment - Azimuth 285°

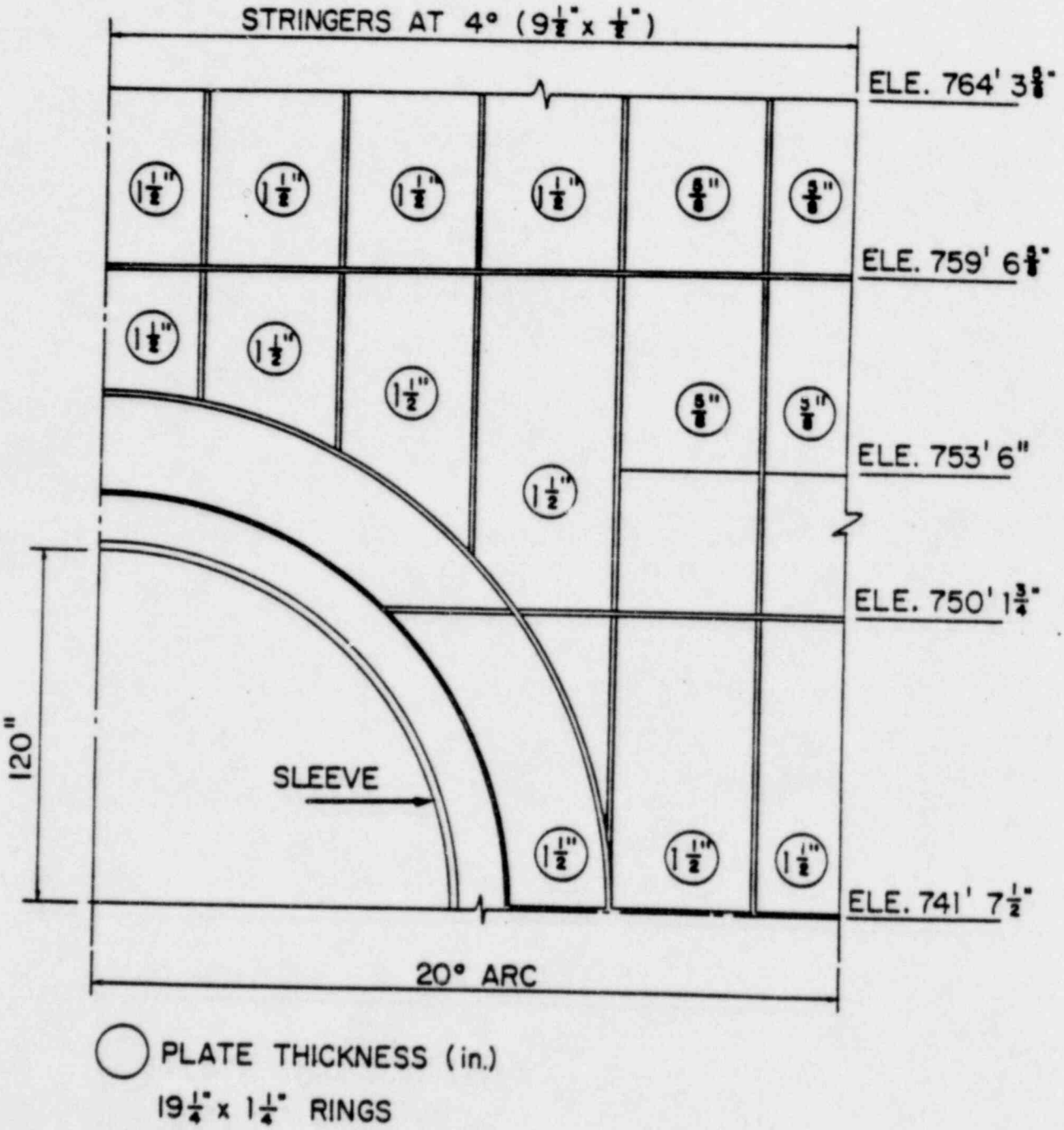

Figure 2.2 Sequoyah Containment Shell Plate Thicknesses

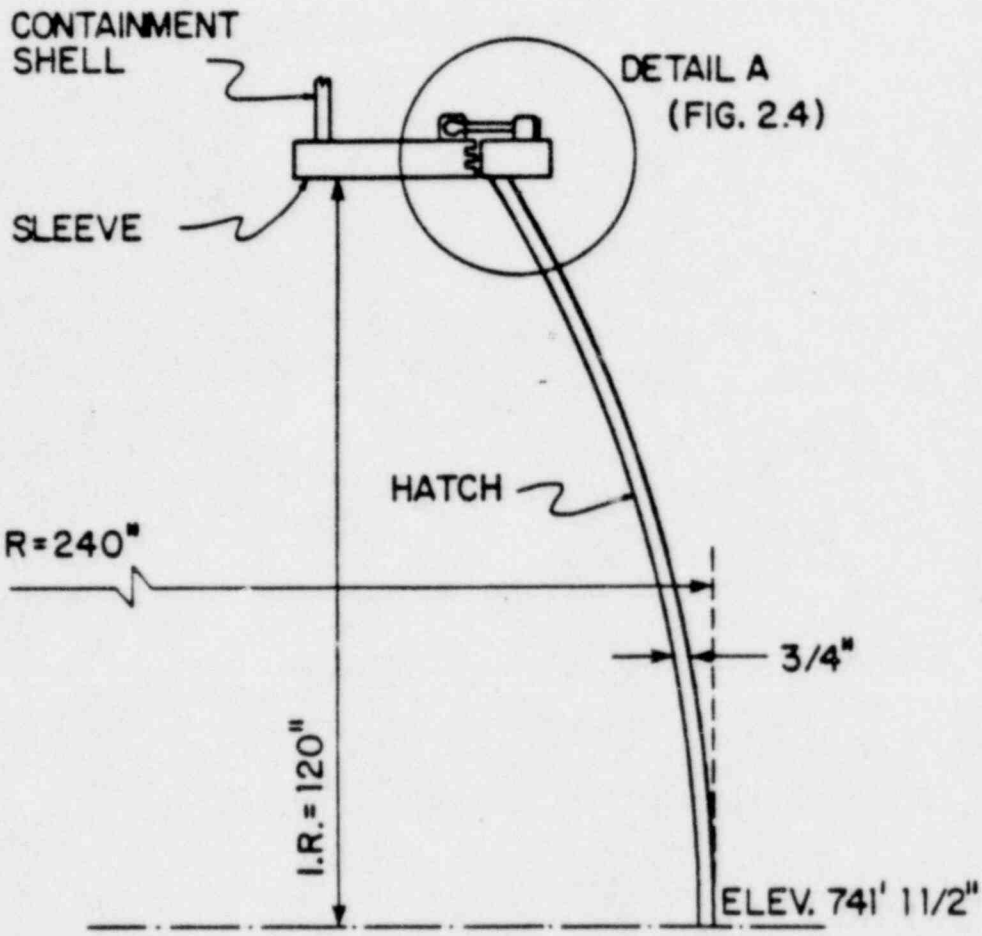

Figure 2.3 Sequoyah Equipment Hatch Elevation

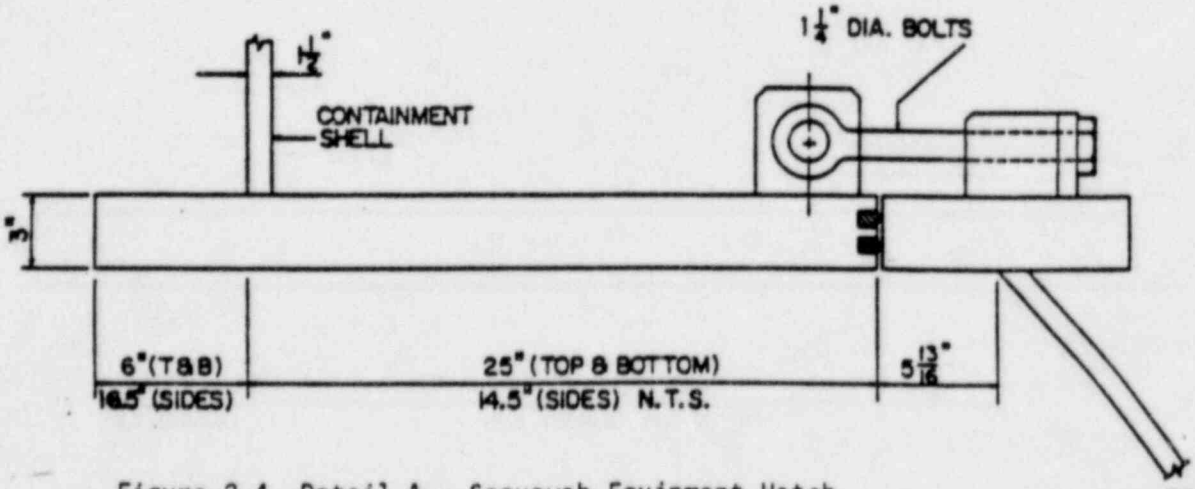

Figure 2.4 Detail A - Sequoyah Equipment Hatch

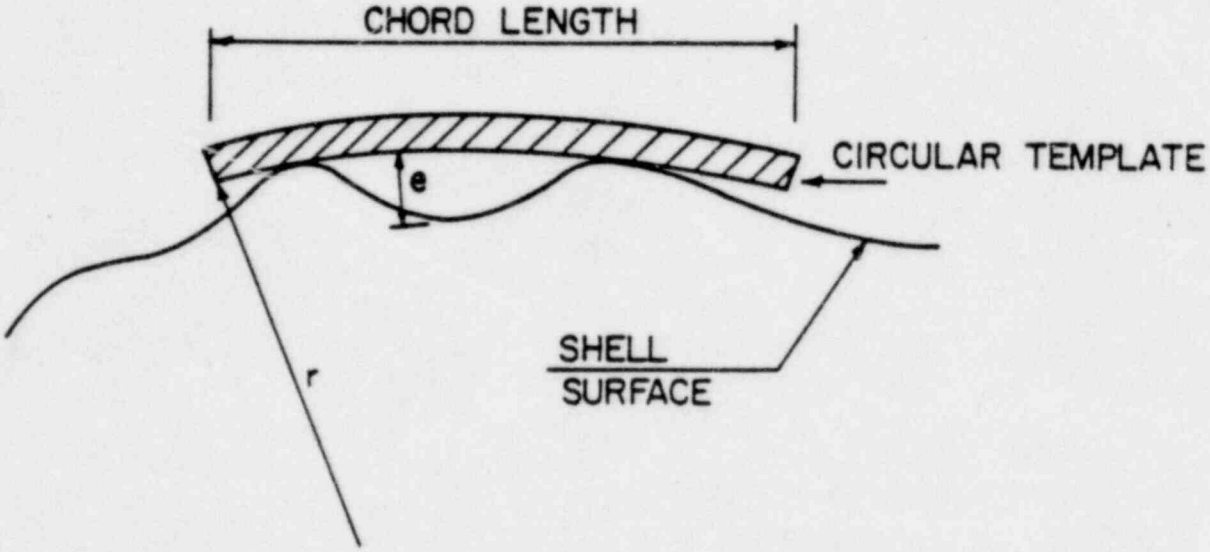

CHORD LENGTH = TWICE THE ARC LENGTH

ARC LENGTH = FIG. 4221.2.2 ASME CODE

e = DEVIATION FROM TRUE SHAPE
FIG. 4221.2.1 ASME CODE

r = INSIDE OR OUTSIDE SHELL RADIUS

Figure 2.5 ASME Tolerance for Shells

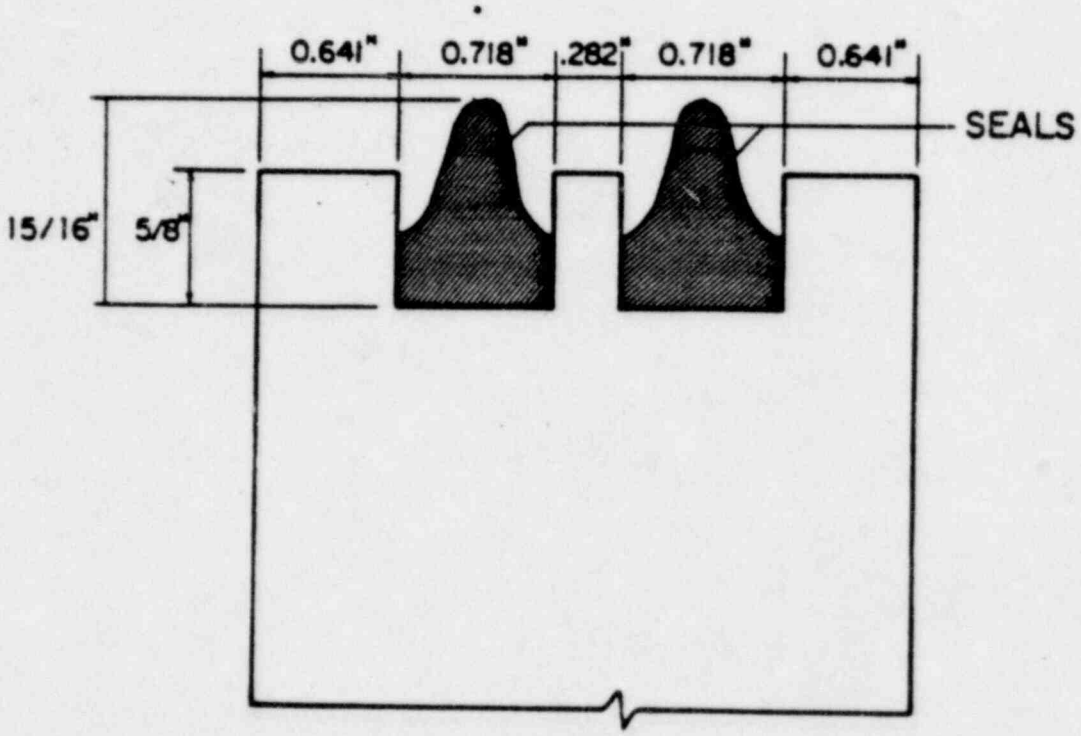

PRESRAY EPDM COMPOUND E 603

	COMPRESSION SET
158°F FOR 22 HRS	14.1 %
7×10^5 RADS AT 120°F FOLLOWED BY 10^8 RADS AT 250°F FOR 72 HRS	13.1 %

Figure 2.6 Seal Configuration

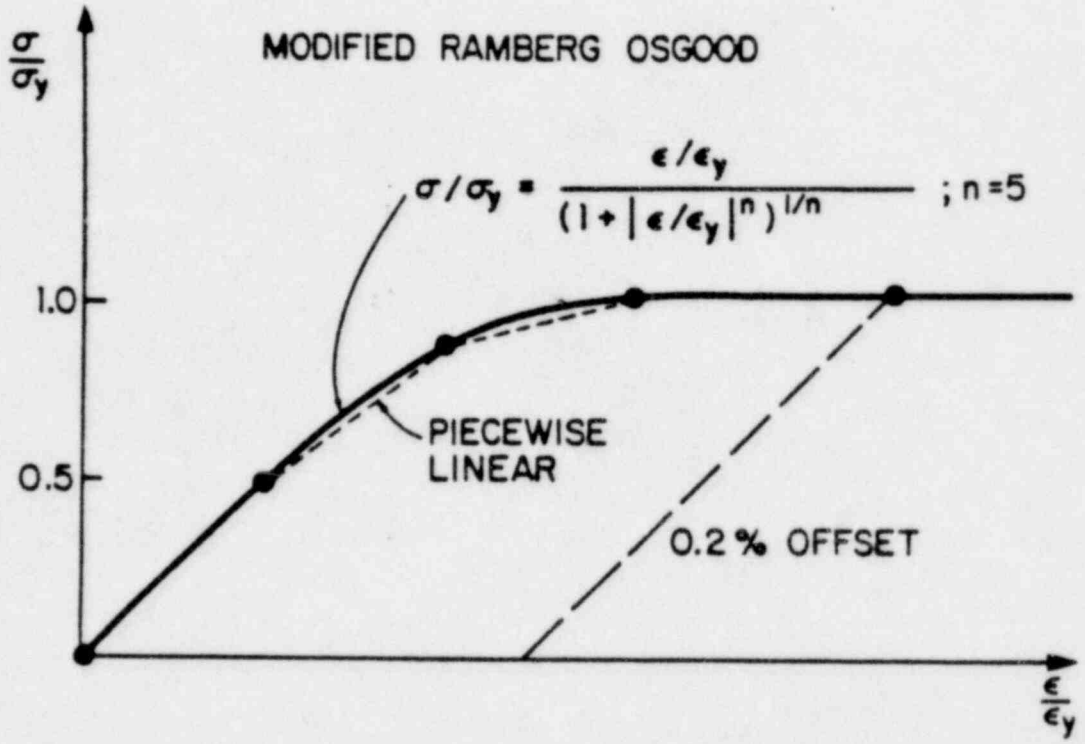

A 516 Gr. 60

PL THICKNESS (in.)	σ_y (KSI)
$\frac{5}{8}$"	49.2
$\frac{3}{4}$"	43.7
$1\frac{1}{4}$"	45.5
$1\frac{1}{2}$"	46.1
3"	40.8

Figure 2.7 Idealized Stress-Strain Curve for Steel

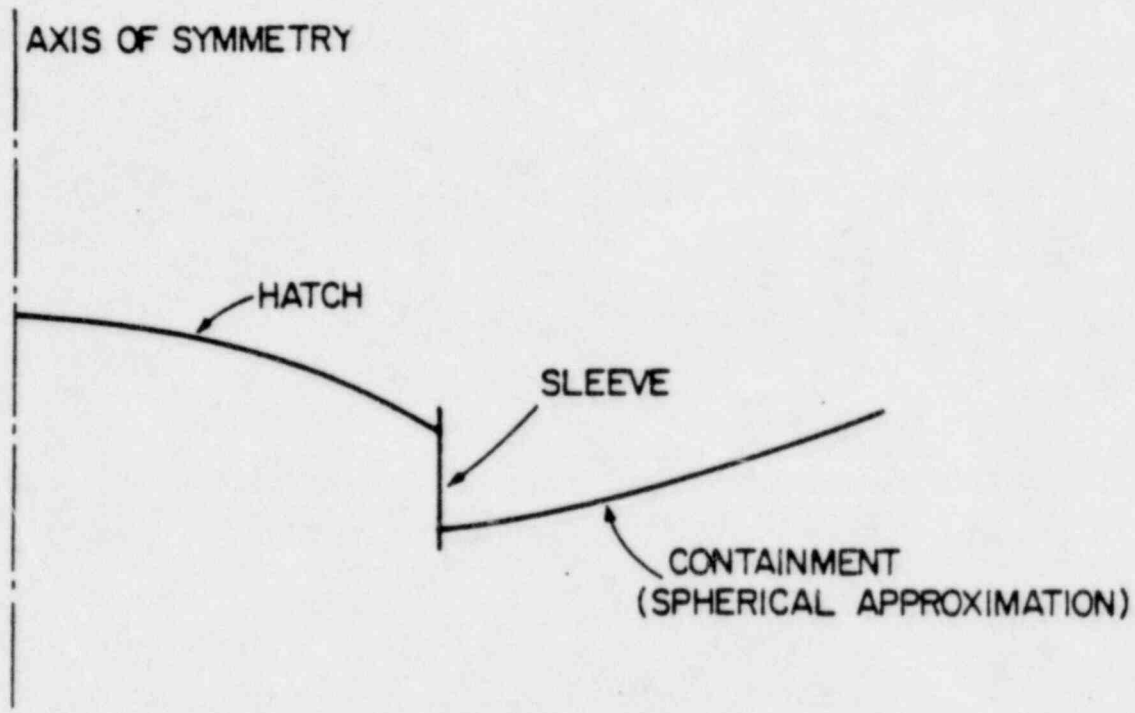

Figure 3.1 BOSOR5 Axisymmetric Finite Difference Model

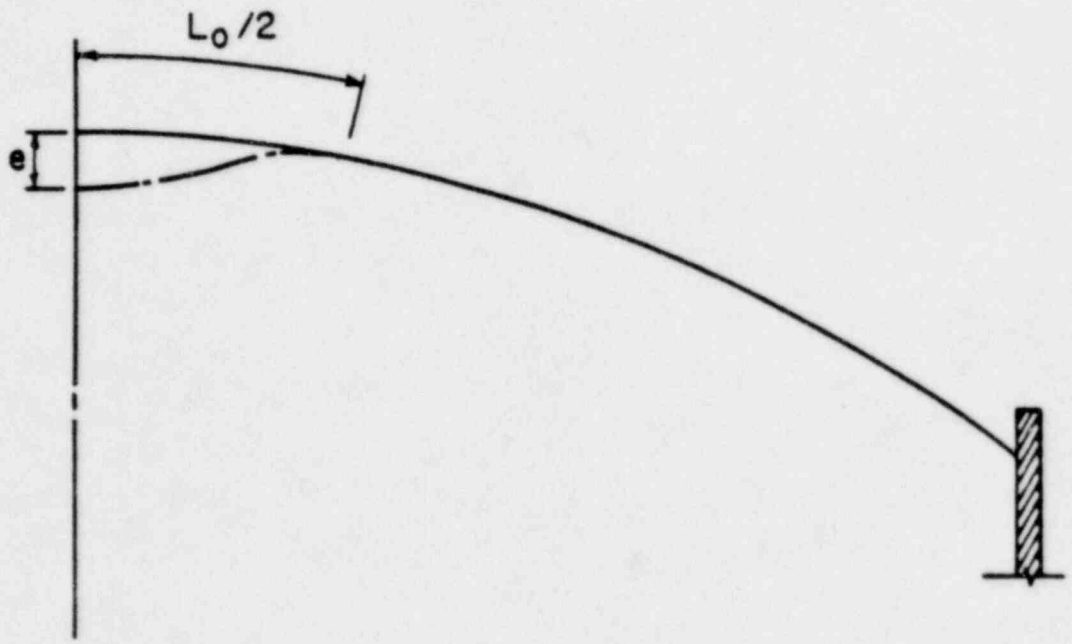

Figure 3.2 Idealized Imperfection at Crown

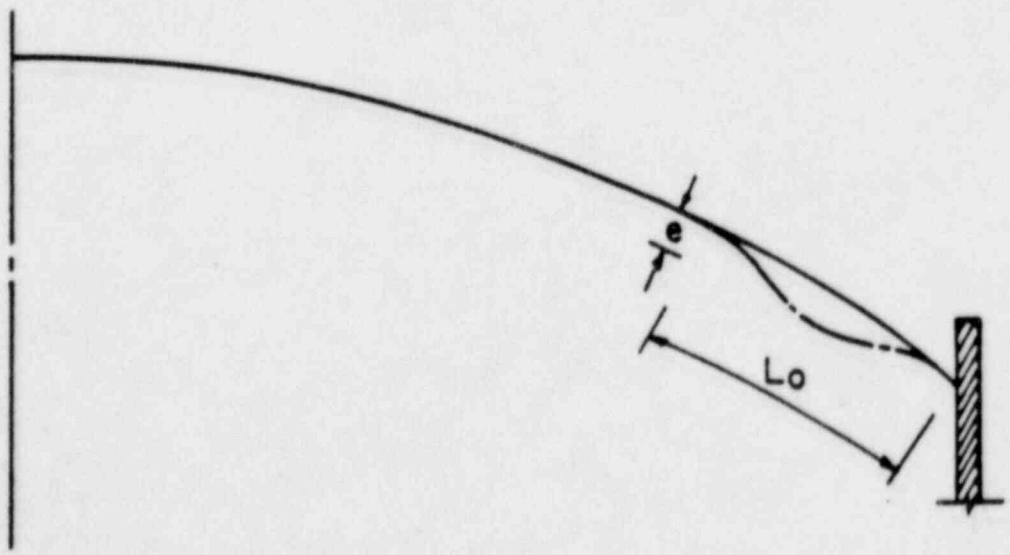

Figure 3.3 Idealized Imperfection at Flange

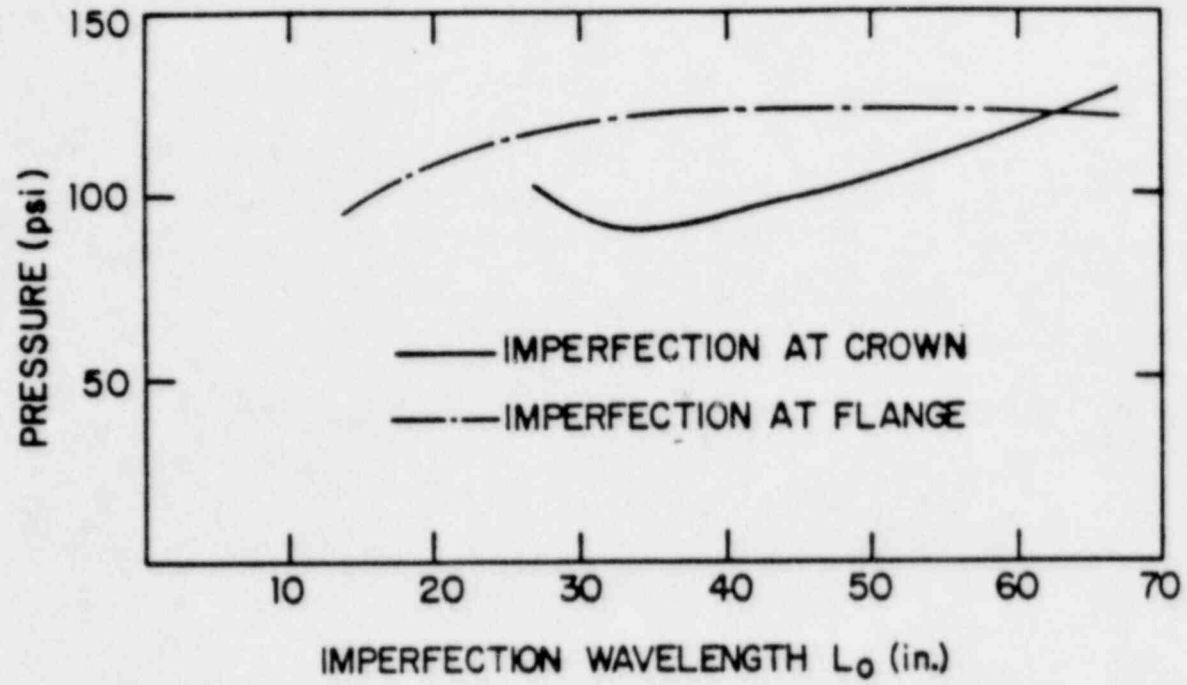

Figure 3.4 Influence of Imperfection Wavelength

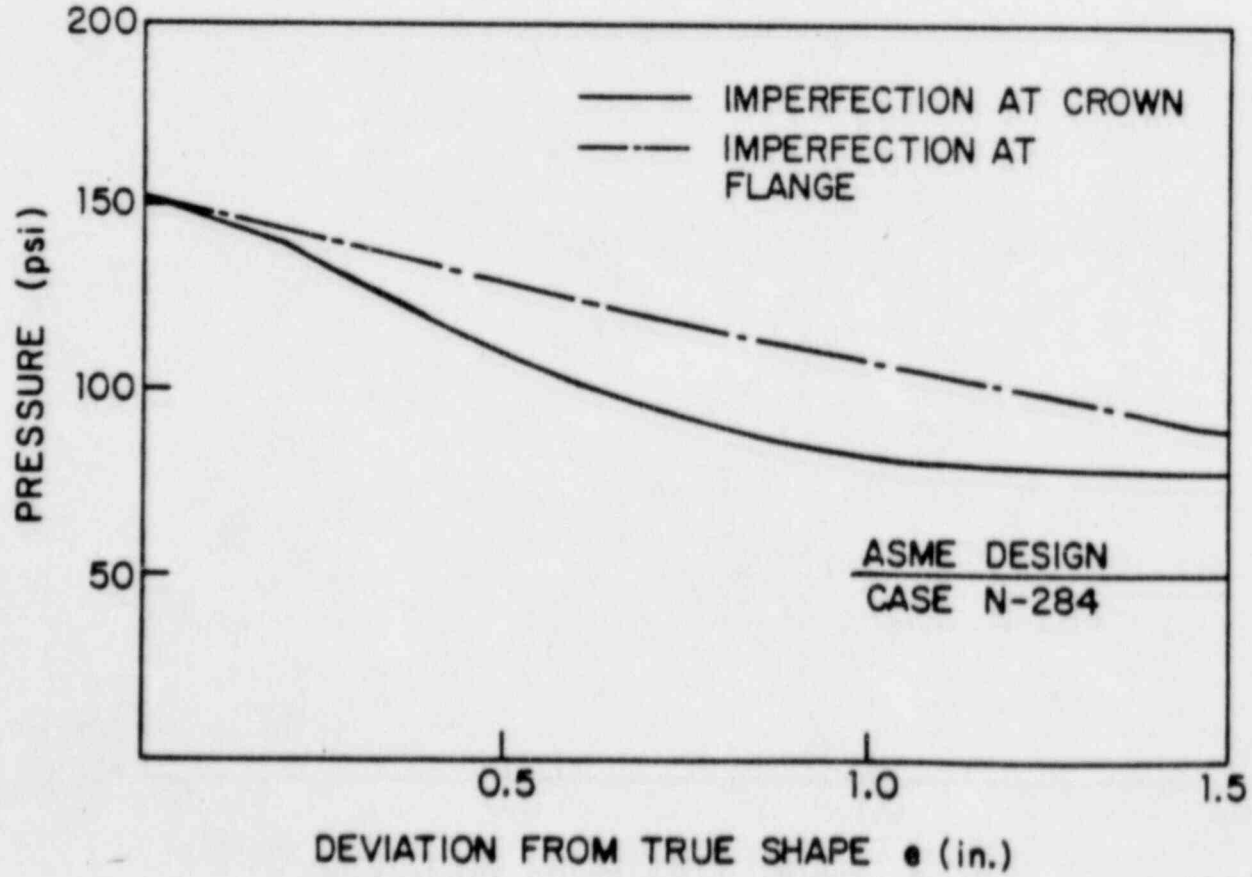

Figure 3.5 Influence of Imperfection Magnitude

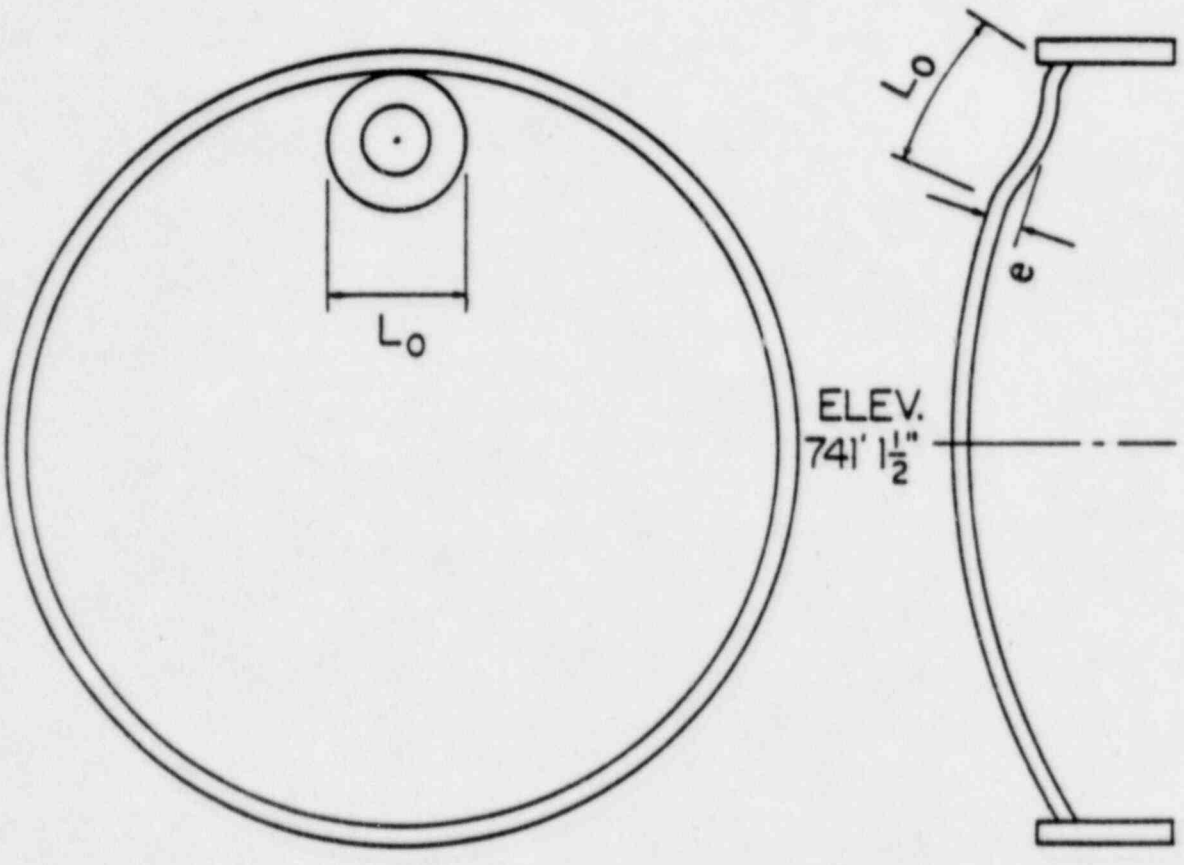

Figure 3.6 Assumed Imperfection for Three-Dimensional Analysis

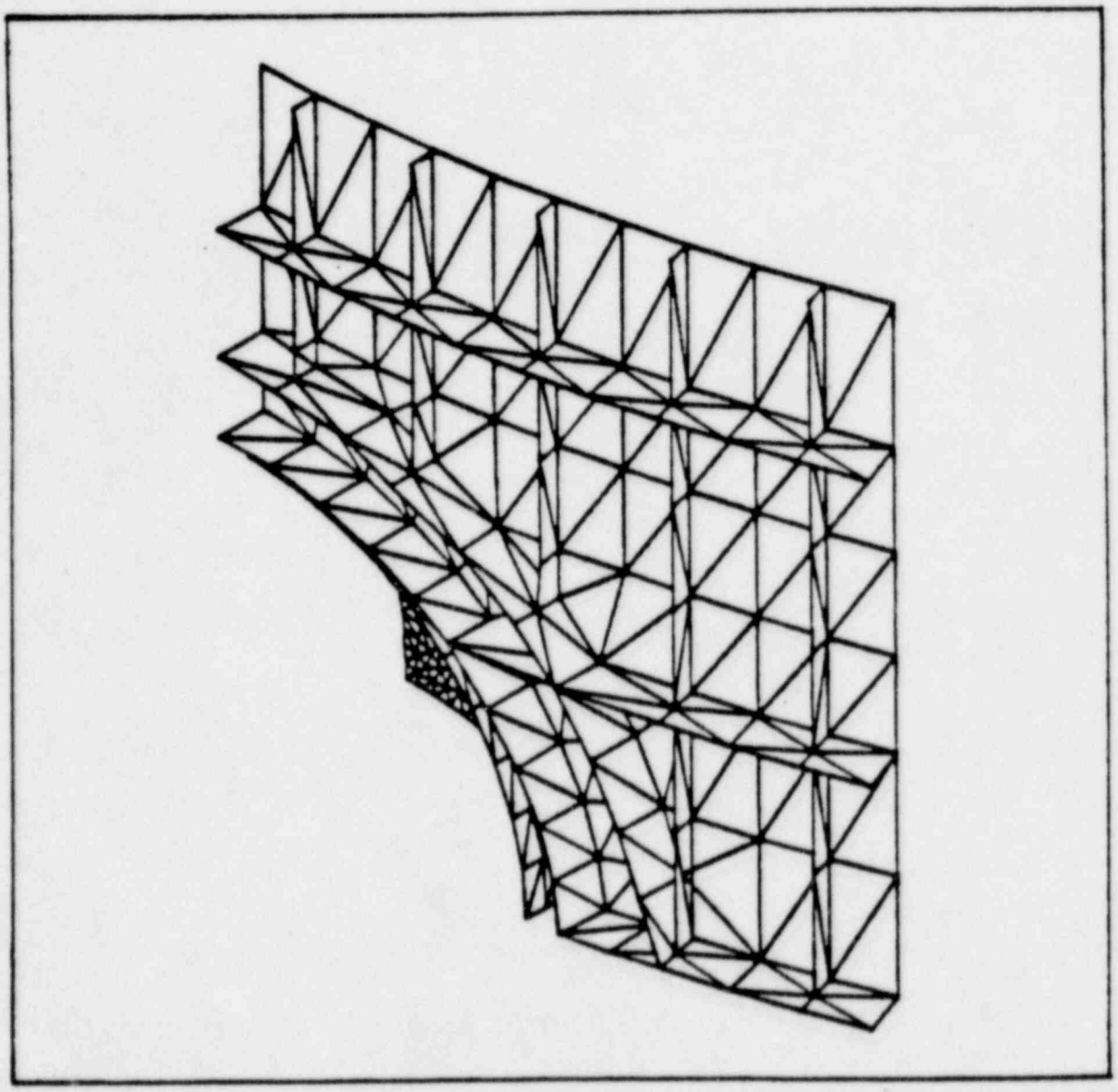

Figure 4.1 Sequoyah Containment Equipment Hatch-Outside View

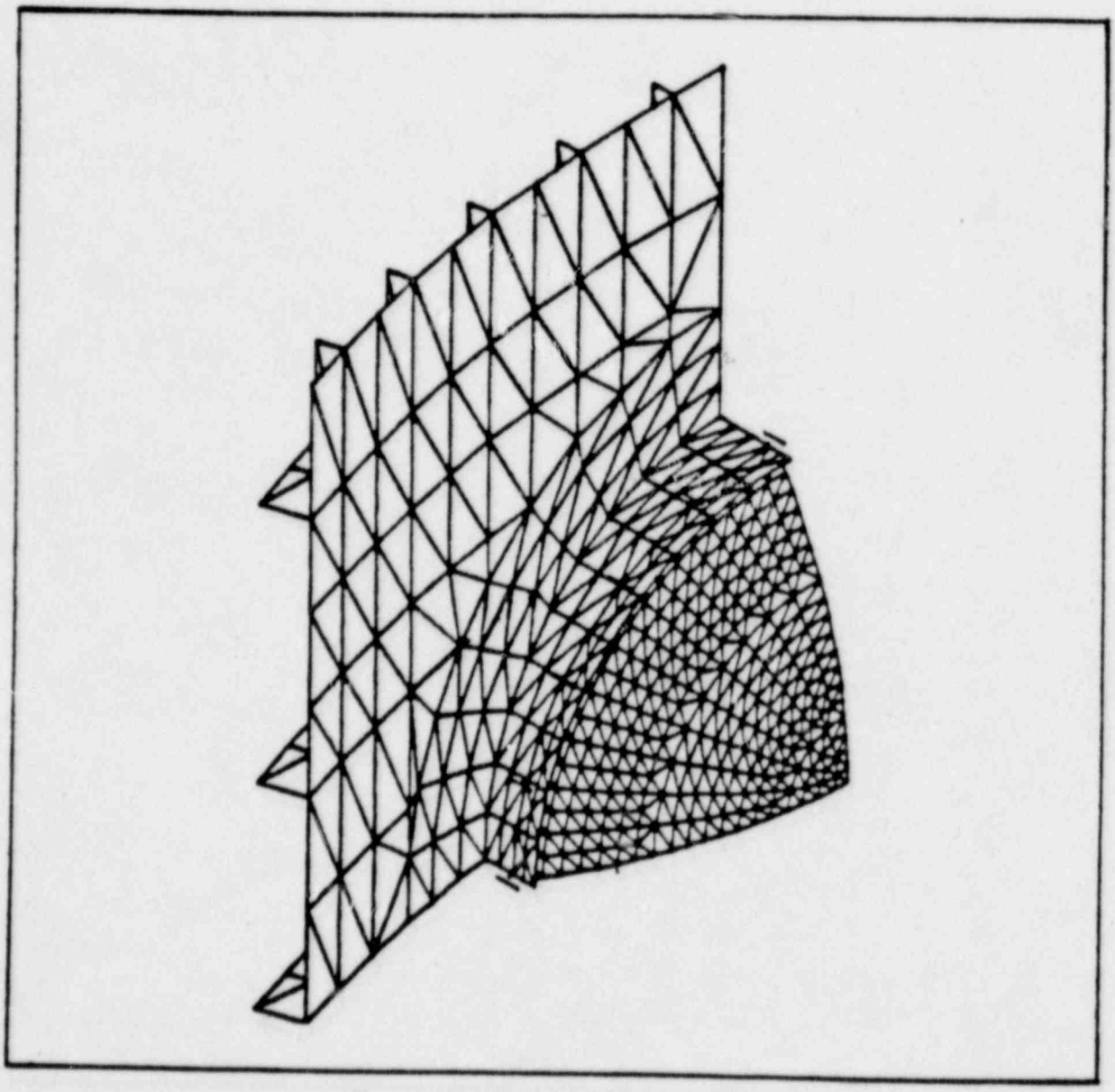

Figure 4.2 Sequoyah Containment Equipment Hatch-Inside View

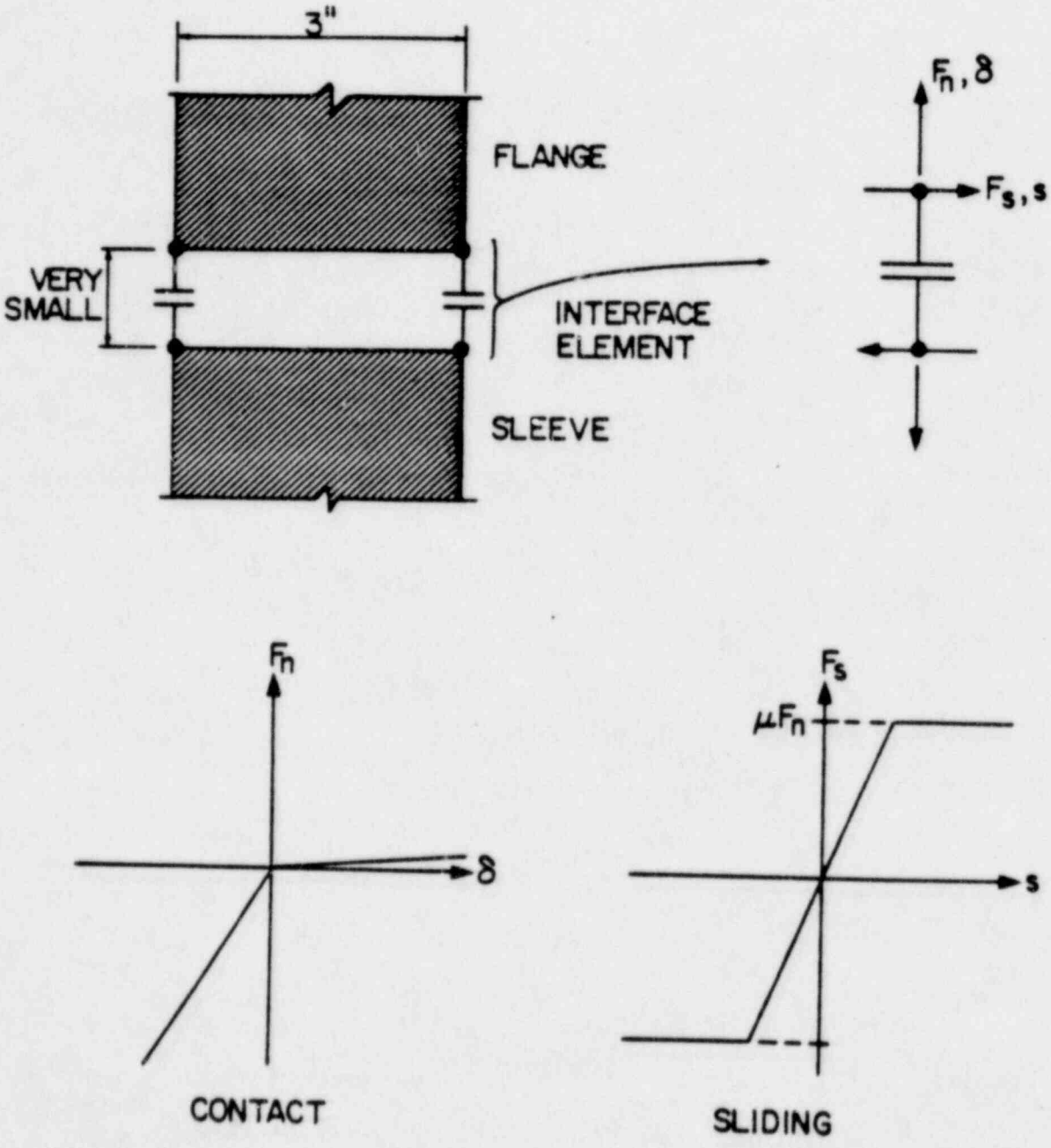

Figure 4.3 Flange/Sleeve Interface Idealization

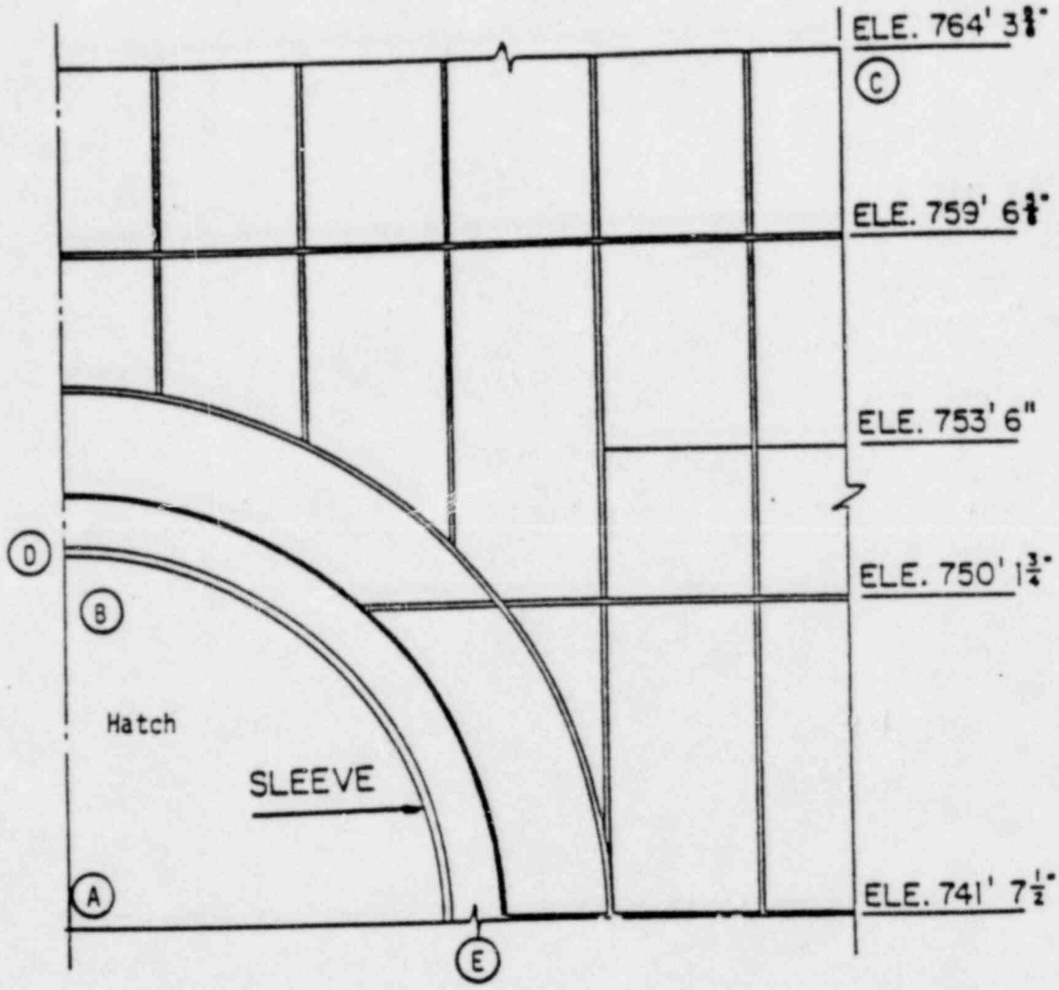

Figure 4.4 Sequoyah Containment Shell Reference Points (see also Figure 4.7 and 4.8)

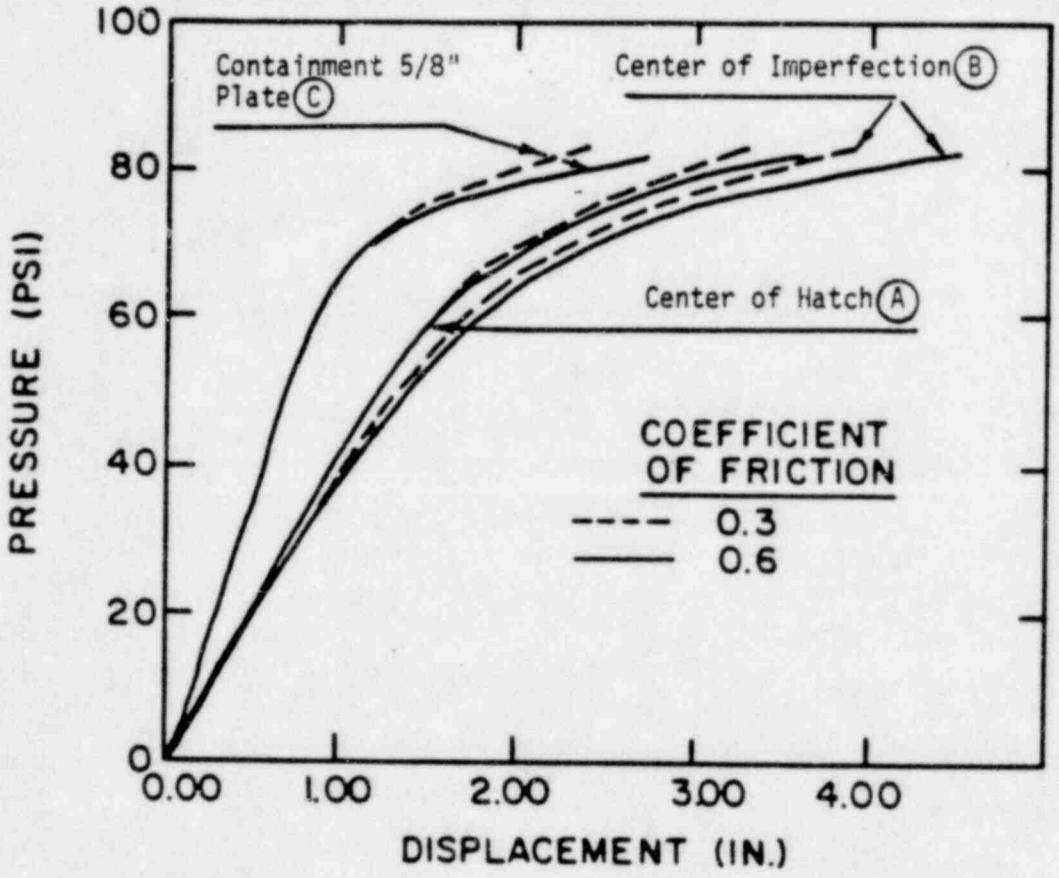

Figure 4.5 Radial Displacement

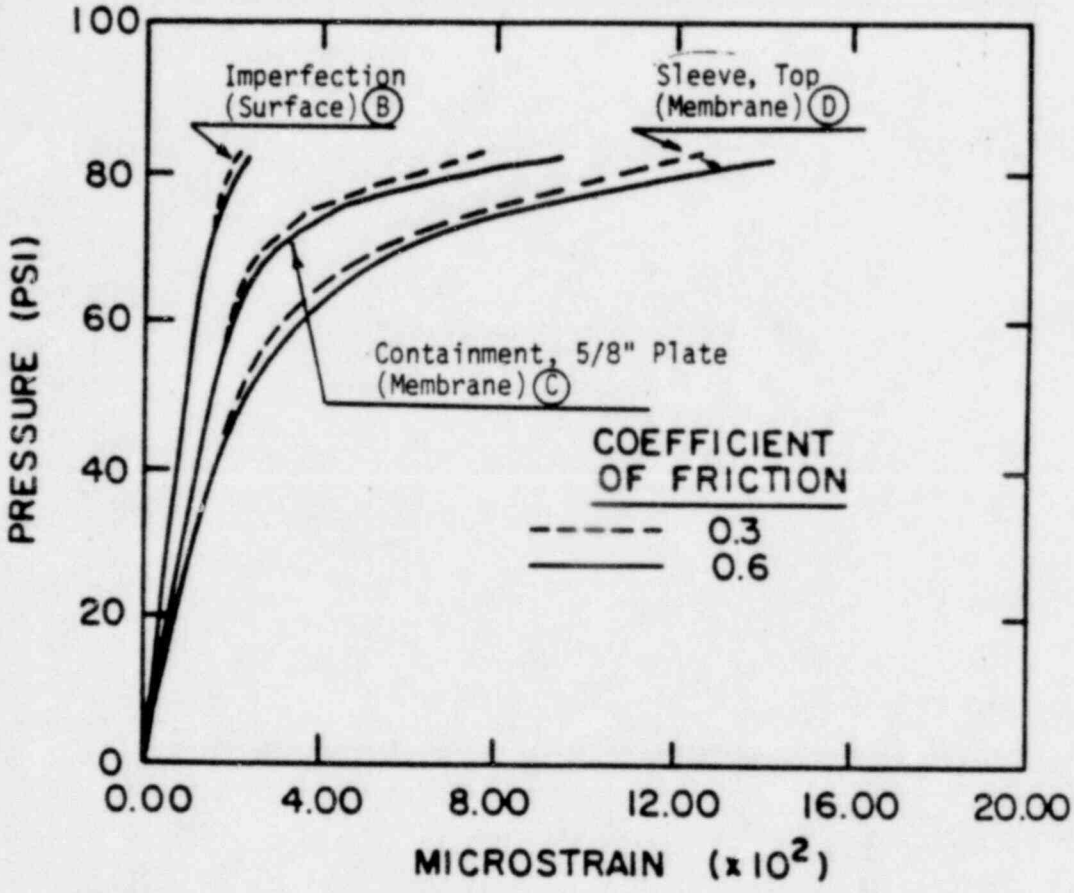

Figure 4.6 Strains at Selected Location in the hatch Model

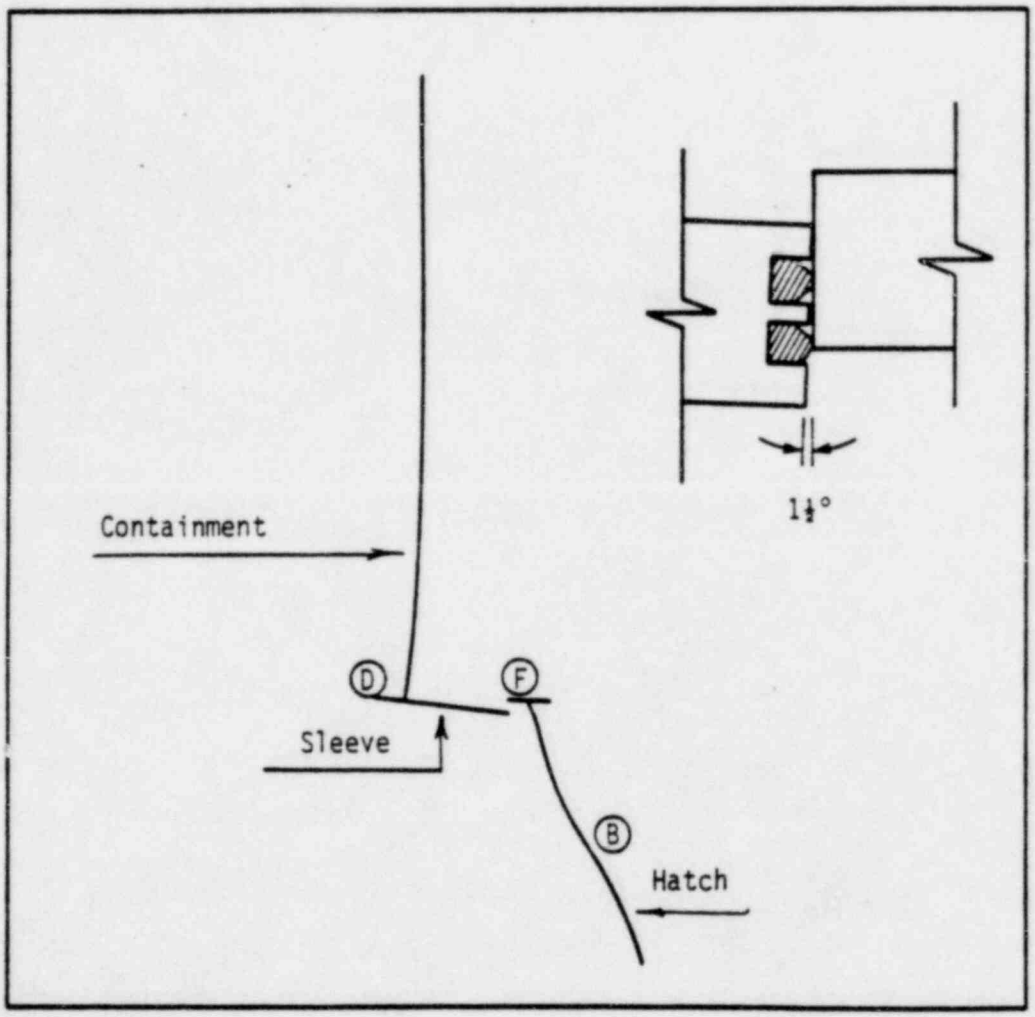

Figure 4.7 Displaced Shape in Vertical Symmetry Plane
(82 psig, coefficient of friction = 0.3)

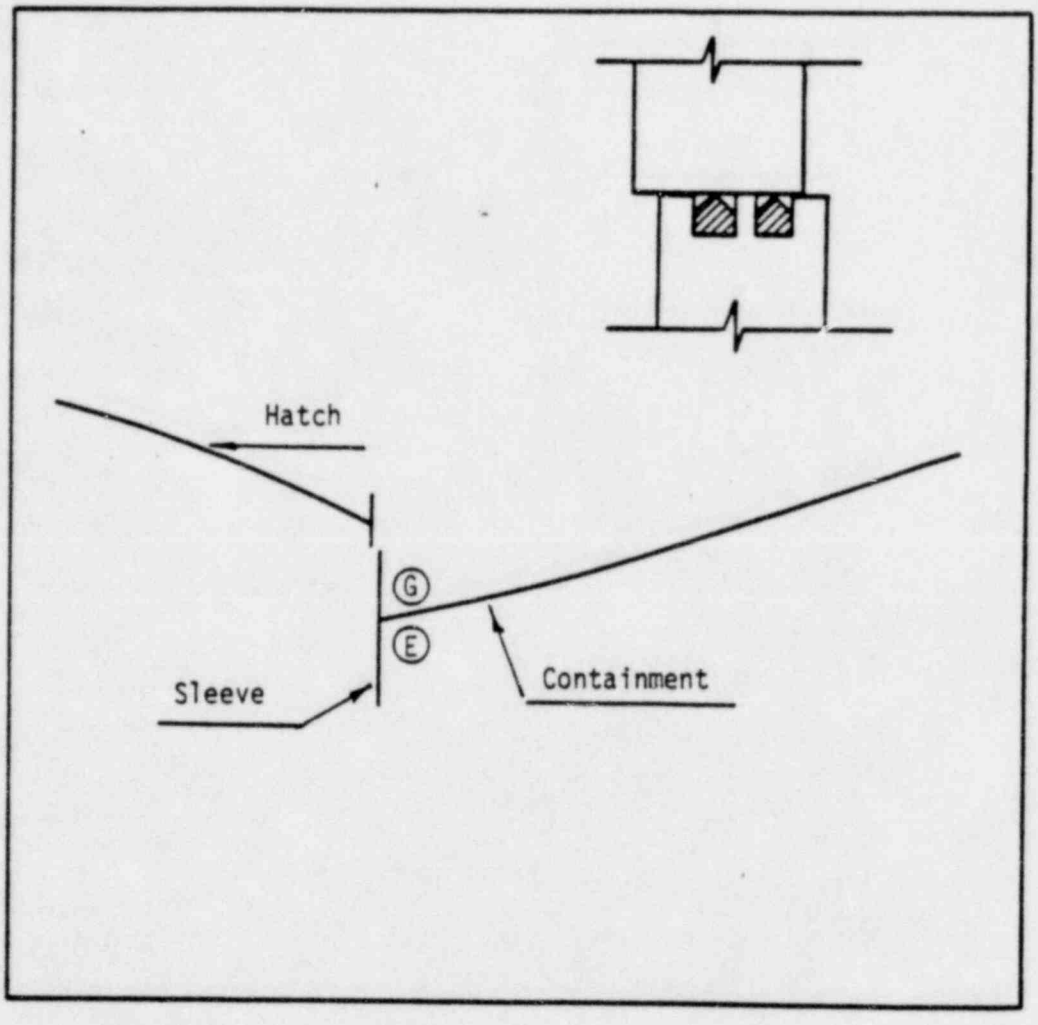

Figure 4.8 Displaced Shape in Horizontal Symmetry Plane (82 psig, coefficient of friction = 0.3)

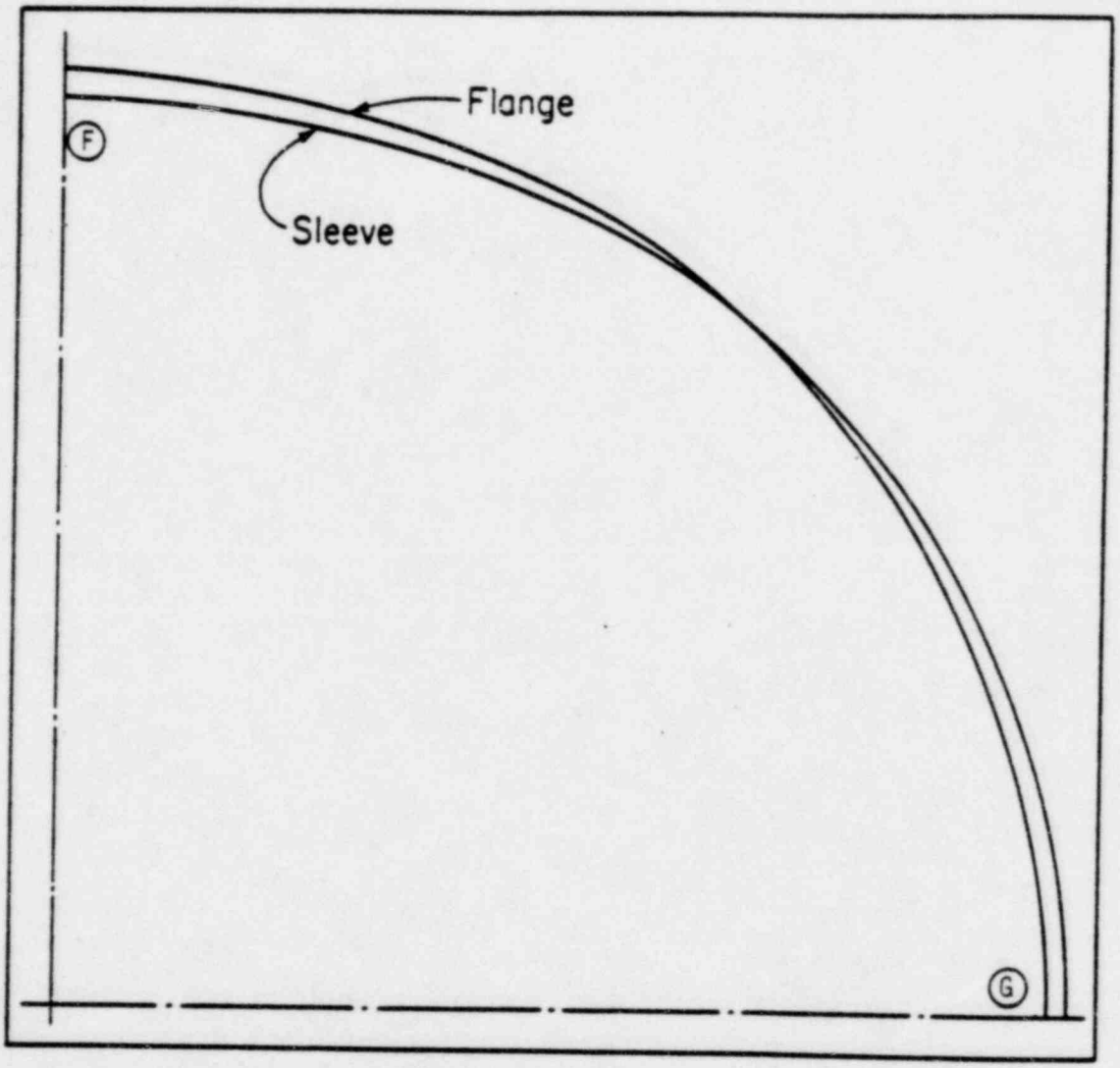

Figure 4.9 Flange/Sleeve Mismatch (82 psig, coefficient of friction = 0.3)

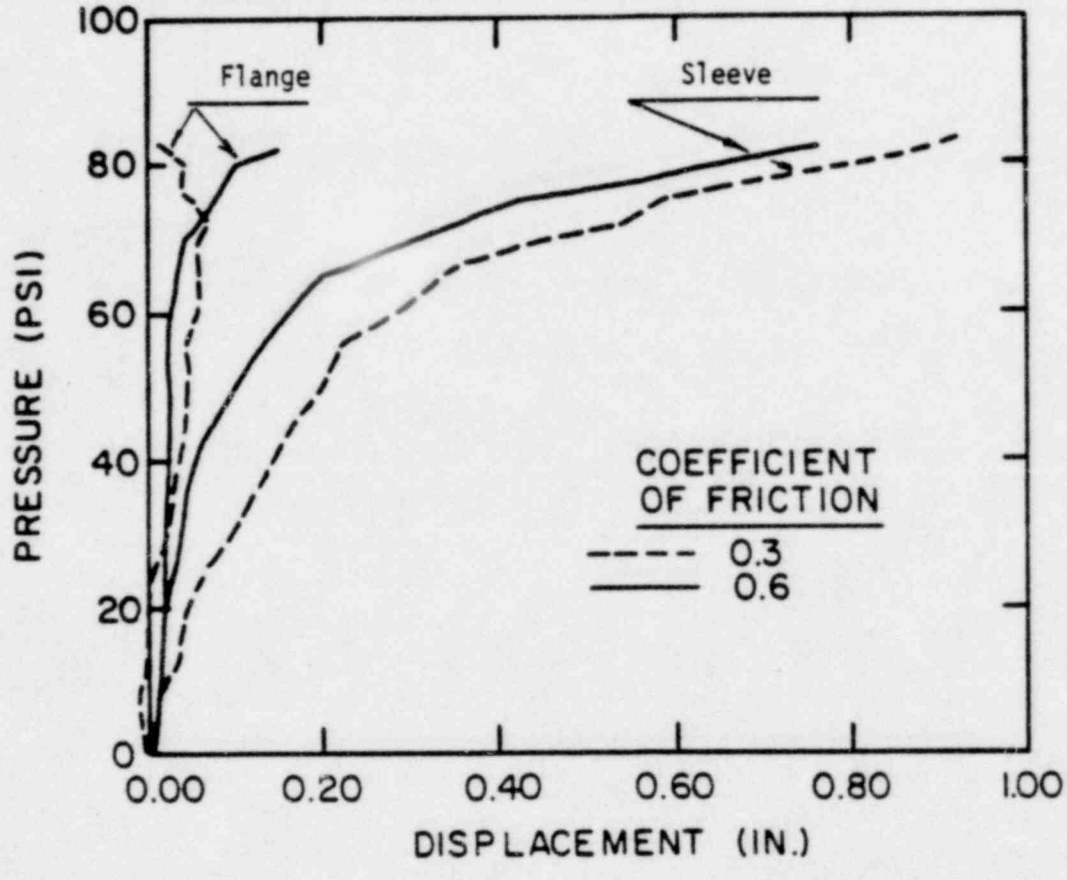

Figure 4.10 Radial Displacement at Seal Surface, Vertical Symmetry Plane, (F)

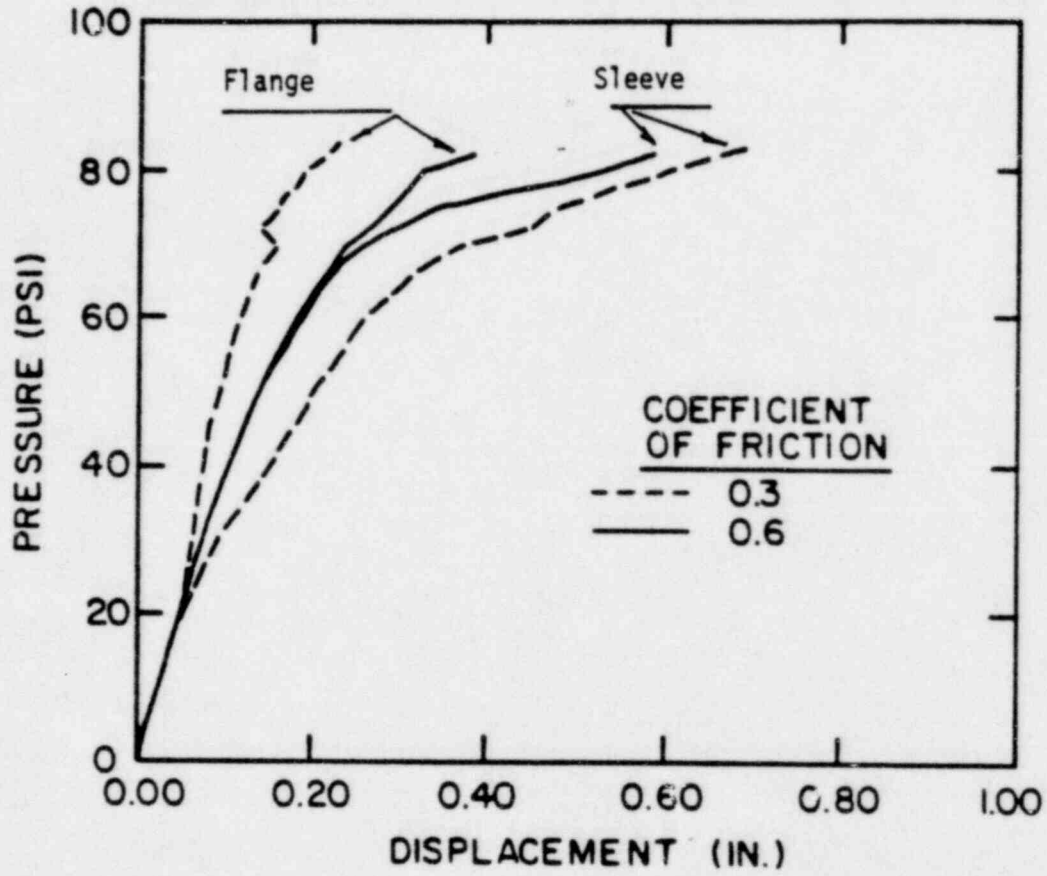

Figure 4.11 Radial Displacement at Seal Surface, Horizontal Symmetry, (G)

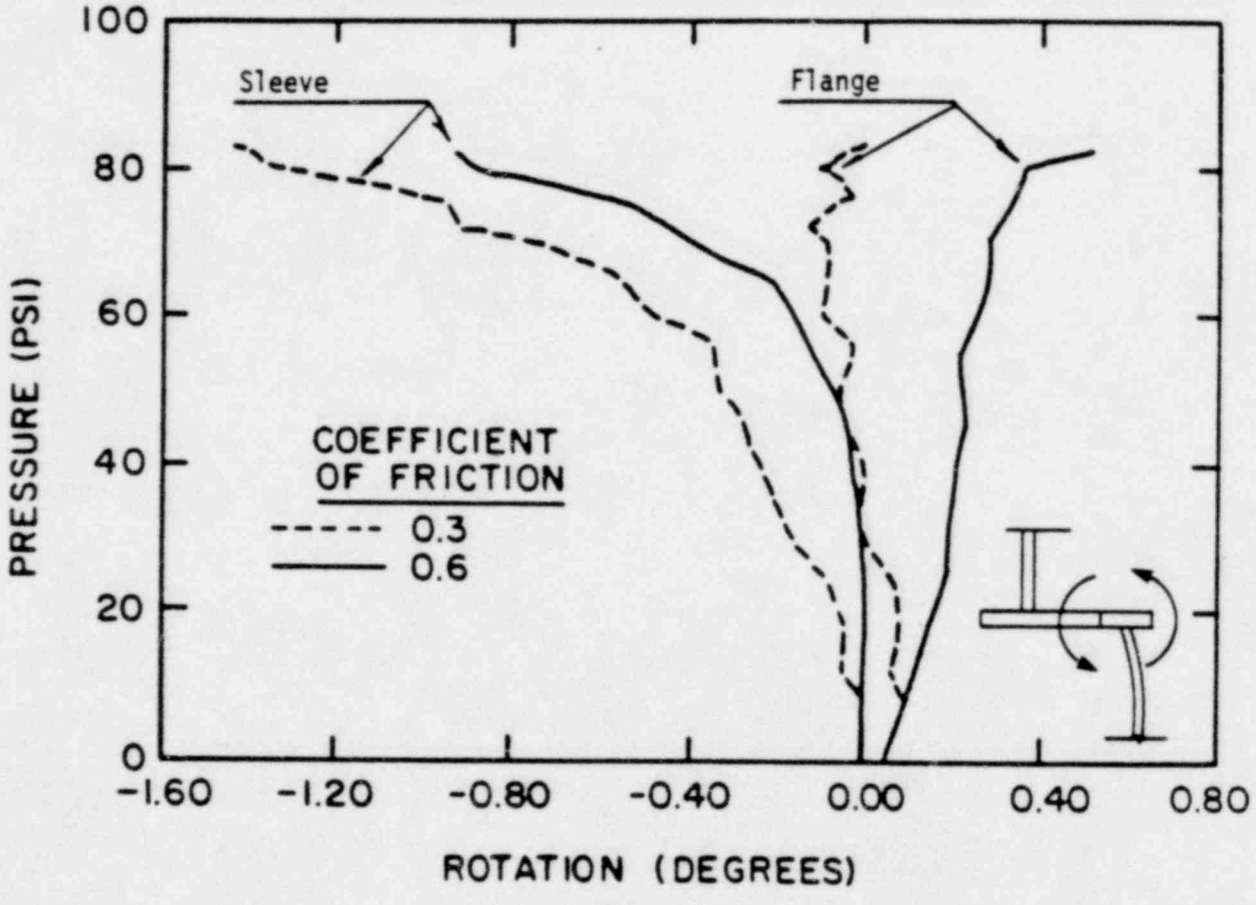

Figure 4.12 Rotation at Seal Surface, Vertical Symmetry Plane

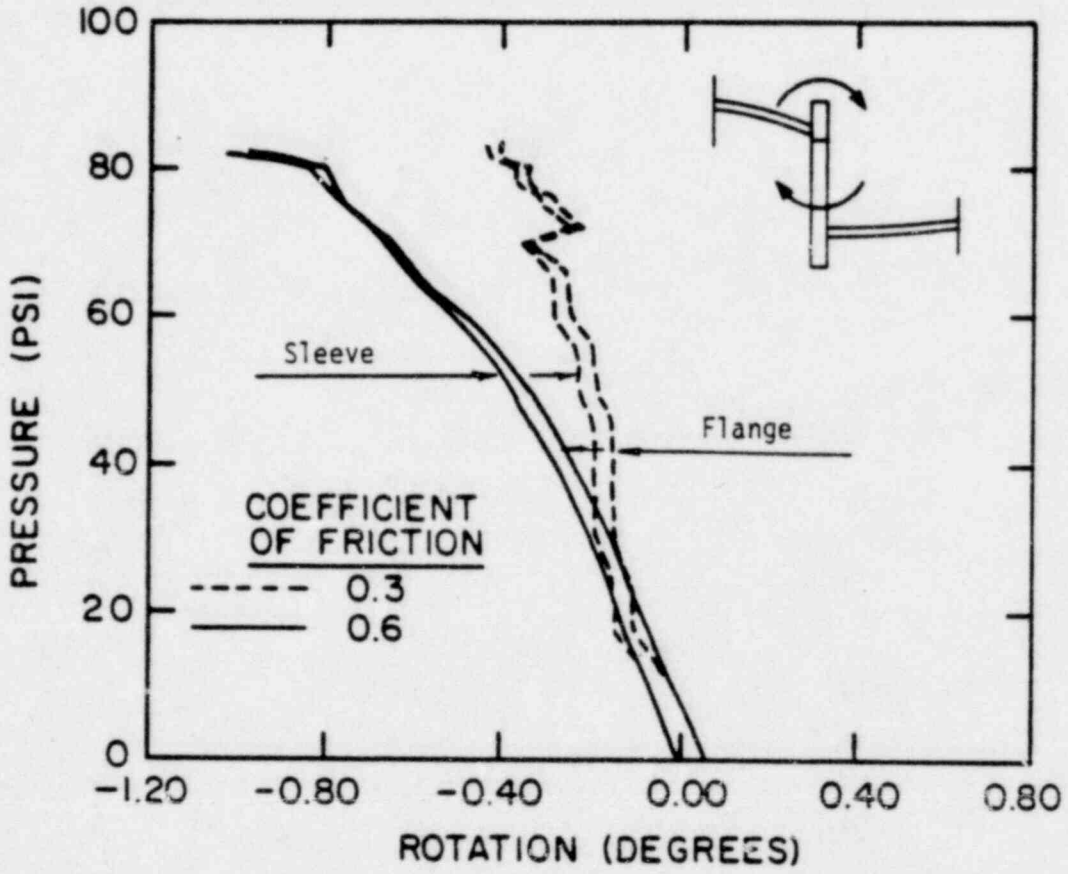

Figure 4.13 Rotation at Seal Surface Horizontal Symmetry Plane

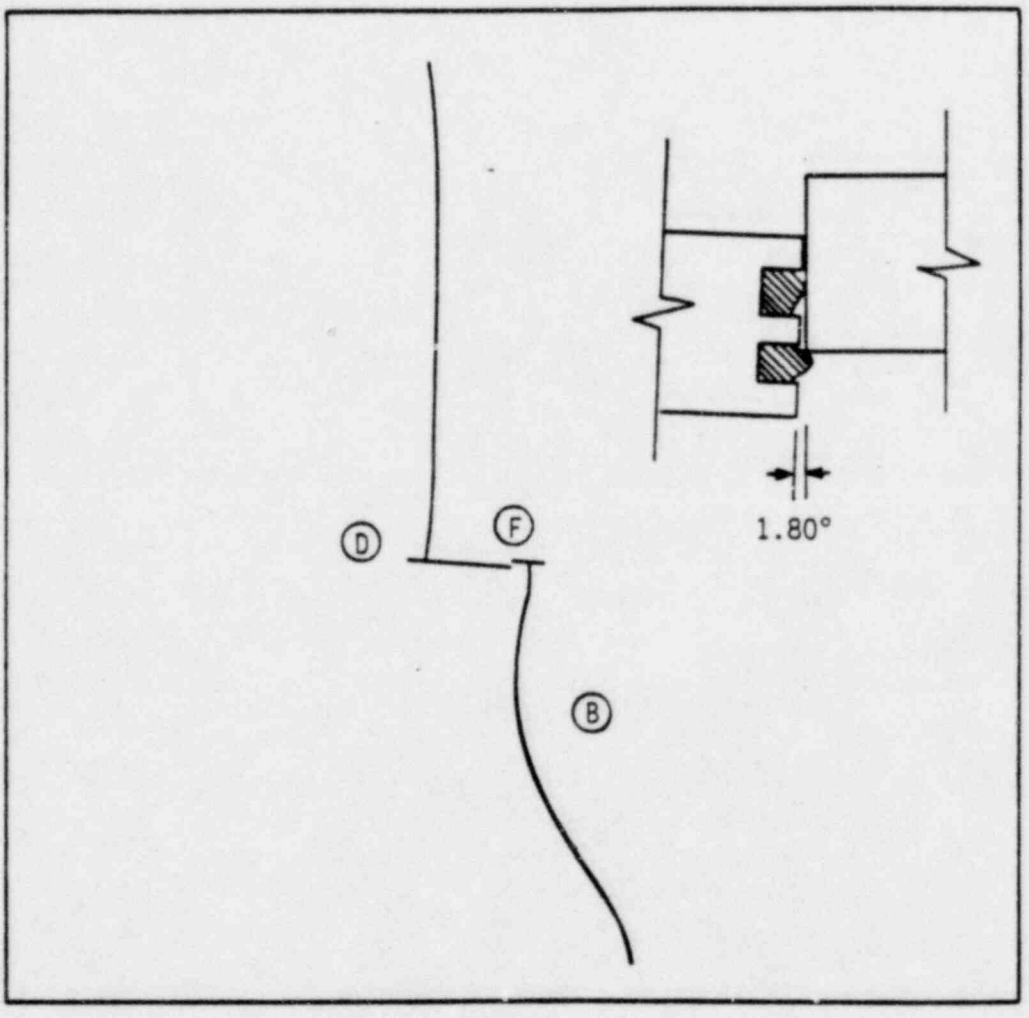

Figure 4.14 Displaced Shape during the Postbuckling process at Vertical Symmetry Plane (90 psig, coefficient of friction = 0.3)